12-2015

EXPERIMENTAL INVESTIGATION OF HEAT LEAKAGE AND AIR LEAKAGE IN DOMESTIC REFRIGERATORS

Shervin Shoai Naini
Clemson University, sshoain@g.clemson.edu

EXPERIMENTAL INVESTIGATION OF HEAT LEAKAGE AND AIR LEAKAGE IN DOMESTIC REFRIGERATORS

A Thesis
Presented to
the Graduate School of
Clemson University

In Partial Fulfillment
of the Requirements for the Degree
Master of Science
Mechanical Engineering

By
Shervin Shoai Naini
December 2015

Accepted by:
Dr. Richard S. Miller, Committee Co-Chair
Dr. John R. Wagner, Committee Co-Chair
Dr. Jay Ochterbeck

ABSTRACT

The optimization of the energy consumption in household refrigerators should consider the influence of the gasket which determines the heat transfer and air infiltration rate. In this research project, engineering methods are developed to evaluate the heat leakage due to the gasket and air infiltration in domestic refrigerators.

In the first study, experimental and numerical approaches are applied to evaluate the gasket heat transfer based on the "Reverse Heat Load Method". The main objective is to find the effective heat leakage with the dimensions of energy leakage per gasket length per temperature difference (W/m.K). An insulated cubic box with a 216,000 cm^3 interior enclosure (60cm x 60cm x 60cm) was designed to accept a matching set of adjoining refrigerator door and wall cuts placed inside the cavity. The door and walls are surrounded by thick insulation material so that only the gasket region is exposed to the ambient environment. A heat source was placed inside the center of the box to create a desired temperature difference between the interior and the ambient. Thermocouples measured the interior and ambient temperatures while six heat flux sensors, mounted on the exposed gasket region, measured the heat flux exiting the box through this region. Two restrictions were imposed with the heat flux sensors to evaluate the heat leakage purely experimentally. The heat flux sensors did not offer sufficient resolution to fully resolve the surface heat flux distribution, and they were incapable of directly measuring the heat flux leaving through the gasket due to its complex geometry. Therefore, Computational Fluid Dynamics (CFD) simulations were necessary to complete the heat flux profile between the

experimental data points recorded by the sensor (the CFD results were supplied by a colleague, Mr. Feng Gao). Accordingly, a two dimensional (2D) simulation was performed to provide a shape profile of the heat flux leaving the gasket region which may be used to fit the experimental data using a "Least Mean Square Error" approach. The estimated heat loss at the gasket region with the original gasket installed on the sample refrigerator was 0.20 W/m.K. Extensive testing with other gaskets showed that their design and materials influenced the heat loss of the refrigerator.

The second study developed a methodology to identify the leaks, to estimate the air infiltration rate, and to calculate the energy loss associated with air leaks in domestic refrigerators. The water drain tube was determined to be the primary air leak source due to the presence of the evaporator fan inside the freezer compartment. In addition, many other leaks with unknown sizes were found through bubble tests about the cabinet. Two identical refrigerators were employed to evaluate the impact of the air loads. One refrigerator remained with its original conditions and the other unit was completely sealed so that there existed a single inlet (water drain tube) and a single outlet (a drilled hole). The intact refrigerator was used to measure the normal operating conditions with respect to the ambient environment (e.g. pressure and temperature differences) to mimic these conditions in the sealed unit. The sealed unit had a hole drilled into the cabinet and the water drain tube remained open to the ambient. The size of the drilled hole was adjusted until the same pressure difference was achieved on the new unit at the same temperature difference. A flow meter measured the air flow through the hole and thermocouples measured the ambient and interior temperatures simultaneously. The energy leakage due to the air infiltration was calculated using the first law of thermodynamics based on two

temperatures and mass flow rates at the inlet and outlet. The actual air infiltration rate was measured and the effective heat transfer rate due to the air infiltration rate was calculated 4.4 Watts. Modeling shows that refrigerators are not under steady state operation. They "breathe" drawing air in during cooling and forcing air out during warming between compressor cycles. A hypothetical perfectly sealed unit is shown to produce forces upwards of 1550 N (350 lbf) on the fresh food door due to this effect alone.

ACKNOWLEDGMENTS

I would like to express my deepest appreciation to my supervisors, Professor Richard Miller and Professor John Wagner. They have kindly assisted me every step of the way, providing insight, guidance and encouragement. I will always be thankful to my advisors for offering me inspiring suggestions and bringing me to a higher level of thinking.

I am grateful to Professor Jay Ochterbeck for reviewing my papers and giving me valuable advice. I am also thankful to him for serving in my committee.

Special thanks to my talented colleague, Mr. Feng Gao, who worked hard on this project to develop CFD model. Working with him was a great learning experience for me and I deeply appreciate the friendship we made over these years.

Thanks to all my friends who made my stay in United States memorable. I would like to give a special thanks to Sara who always supported and encouraged me in all of my pursuits. I would also like to warmly thank my best friends who proved that true friendship is neither a function of space nor time.

And above all, I would like to express my gratitude to my parents and my sister; without unconditional love and support of whom, nothing I have ever accomplished in my life would have been possible. I am really lucky to have them be my family.

TABLE OF CONTENTS

Page

Table of Contents (Continued) Page

LIST OF FIGURES

List of Figures (Continued) Page

List of Figures (Continued) Page

LIST OF TABLES

1. INTRODUCTION

Over the last decades, domestic refrigerators have been known as one of the significant energy consumer devices in home applications. A lot of research has been conducted to develop methodologies to study weaknesses in existing designs of domestic refrigerators in order to achieve a significant reduction in the power consumption. There are some papers [1, 2, 3] that suggested design modifications to improve the performance of refrigerators. However, not many publications are available on the magnetic door gasket section; although there is a significantly high percentage of the heat loss attributed to the gasket section. Hasanuzzaman [4] studied the power consumption of a refrigerator experimentally due to cabinet load variations, such as cabinet water load and water pan area, and the changes of environmental conditions like ambient temperature, and thermostat setting. He has mentioned that the refrigerator power consumption in the most optimized case is 53 percent lower than the worst case conditions. Twenty nine percent of the heat loss occurred specifically through the gasket region. Boughton [5] determined the heat loss at the edges of the door gasket, called edge loss, to be about 30 percent of the total thermal load. EPA's Air and Energy Engineering Laboratory [6] reported that the heat loss due to the gasket region varies between 10 to 30 percent based on the refrigerator model, gasket effectiveness and ambient conditions. They also found that gasket infiltration results in a significant portion of energy loss in domestic refrigerators. Hilligweg [7] and Tao and Sun [8] designed different test configurations based on the "Reverse Heat Load Method" in order to evaluate the total heat loss attributed to the gasket section. They both conclude that the heat loss occurred due to the gasket region is around 13 percent of the total thermal

load. Bansal [9] studied reducing the energy consumption in five major household applications including fresh-food and freezer compartments. He named magnetic door gasket as one of the main weaknesses resulting in reducing the energy efficiency in refrigerators. He remarks that the magnet material, surface conditions, gasket flexibility and gasket compressibility are the primary factors which influence the refrigerator performance. Figure 1.1 shows a 2D cross section of designed geometry for CFD simulation and a 2D cross section of the real gasket installed on the sample refrigerator.

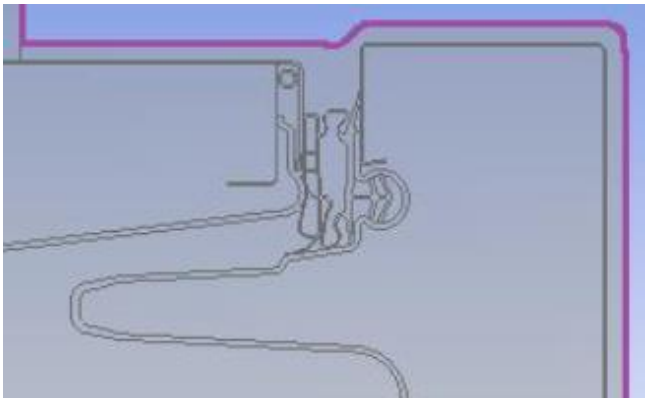

(a)

(b)

Figure 1.1: Magnetic door gasket cross section. (a) 2D geometry of the gasket. (b) Real gasket cross section

There are many schemes proposed in order to investigate and evaluate the heat transfer of household refrigerators. Some researchers have focused on computational and numerical analysis, while others have executed experiments to predict the heat transfer characteristics in domestic refrigerators. Sim and Ha [10] analyzed and quantified the heat loss of the refrigerator by implementing the "Reverse Heat Load Method". They employed a heater to add energy, a voltage regulator to control the heater input power, thermocouples to measure temperatures, and a data acquisition system to record the measured temperatures on the computer. The refrigerator was placed inside a controlled temperature and humidity chamber for about 20 hours of heating to keep the environmental conditions consistent. The authors highlighted that 20 hours is the required time for achieving a steady state condition for this sample refrigerator with the provided conditions. It is also mentioned that mounting several thermocouples in different locations within the cabinet is necessary in order to obtain an accurate temperature contour from the cabinet which is technically required to evaluate the interior temperature at different locations. They concluded that the interior temperature difference with respect to ambient temperature has a nearly linear relationship with the heat input. Kim [11] studied the heat transfer near the magnetic door gasket with the aid of numerical analysis by taking advantage of running CFD software, FLUENT. He also took some temperature measurements experimentally to evaluate the computational results. Thus, the heat transfer characteristic for a 2-D geometry of a gasket region was investigated under 3 different circumstances to figure out which condition leads to the actual final temperatures measured experimentally. However, this approach has some weaknesses. First of all, it is assumed that the heat transfer coefficient

is constant over the gasket region which is not true in real operation conditions. Also, they've considered the incoming air flow is constant which limits its applicability.

The Ventilation Measurement Technique (VMT) is widely used to estimate the air infiltration in buildings, HVAC systems, open refrigerated displays and household refrigerators [12, 13, 14]. The main advantage of applying this method is determination of the overall ventilation rate through a simple calculation. The Trace Gas Technique (TGT) is named as one of the most reliable and accurate procedures for measuring the air infiltration rate [15]. The air infiltration through the gasket in domestic refrigerators was investigated by Huelsz [16]. The approach is injecting trace gas into two separate refrigerator units: one with the real condition as a baseline experiment and the other with the gasket perfectly sealed. The selected trace gas, CO_2, is being injected into the units through the water drain tube until a desired CO_2 concentration is reached inside the cabinet. Afterwards, the concentrations of CO_2 are recorded from each unit as a function of time until the gas concentrations approach to a certain value. However, the researchers did not consider the real interior pressure over the operation condition. According to the paper, the pressure difference between the ambient and interior was not measured over the experiment in spite of the fact that the interior pressure was increasing while CO_2 was being injected into the cabinet and it might have affected the results. Also, the ducts between the freezer and fresh-food compartments were sealed which influenced the normal air flow paths inside the cabinet. The author also attempted to quantify the total thermal loads due to the gasket based on quasi-one-dimensional theory in which thermal coefficients were evaluated experimentally and numerically. Afonso and Castro [17] also applied the TGT to the domestic refrigerator to evaluate air infiltration rate in domestic refrigerators. The

paper measured and compared the air leakage through one new and one old gasket installed at a time on a sample refrigerator. They found the air turnover is 1.1 times per hour through the freezer compartment and 2.1 times per hour through the fresh food compartment while a new gasket is installed on the units. These values increase to 12.7 for the fresh-food cabinet and 6.7 for the freezer compartment with old gaskets. The total loss reported for the new gasket, 3.28 W, is approximately 7% of the compressor power consumption averaged over an hour of operation, or approximately 3% of the compressor power consumption during operation.

1.1. Reverse Heat Load Method (RHLM)

The Reverse Heat Load Method (RHLM) forms the basis for much of the present work. It is an experimental setup in which a heat source is placed inside a refrigerator which is itself generally put into a controlled temperature - humidity chamber. The heating element is directly wired to a variable power supplier (VARIAC) to adjust the inner air temperature by adding heat within the unit. The interior temperature distribution is not entirely uniform, so the unit is instrumented with a number of thermocouples mounted on different locations in order to obtain an accurate temperature profile from the interior. Also, the ambient temperature is being monitored by an additional thermocouple placed outside the unit. There is always heat flux travelling through the walls of the unit due to the presence of temperature difference between the interior and ambient. Heat flux sensors are capable of being installed on any desired flat (and some curved) surfaces of the unit for taking heat flux measurements. This experimental setup gives enough control to generate

a desired temperature difference between the inner air and ambient temperatures by adjusting the variable power supplier connected to the heater. However, attention should be paid to reach a steady state condition before getting any temperature or heat flux measurement. Suitable time for reaching steady state condition depends on the design conditions. Some researchers [8, 10] state that 20 hours is sufficient to achieve steady state conditions. In this study, we plot the running time average for the temperature and heat flux to identify the steady state conditions:

$$F(t) = \frac{1}{t}\int_0^t P(t)dt \tag{1.1}$$

Note that the reverse heat load method does not have the capability of investigating the compressor or evaporator operation performance. This method is a simplified model which is widely used to study the heat transfer characteristic of a refrigerator cabinet. It has been used to obtain the heat transfer coefficient for the walls, doors, gasket or the divider between the freezer and fresh-food compartments [5, 10, 18].

1.2. The Objectives of Present Study

Evaluation of the "gasket heat leakage" and the "refrigerator air infiltration" are the primary purposes of conducting the presented research. We are seeking to develop a feasible and reliable methodology to evaluate the gasket heat leakage, estimate the air infiltration rate and its associated heat loss for a sample domestic refrigerator.

Based on definition, the gasket heat leakage is evaluated in the unit of energy leakage per unit time, per unit length, per unit temperature difference across the gasket (e.g. W/m.K). The pattern of the gasket and the presence of the "hot loop" over the circumference of the

freezer cabinet are predicted to be the significant parameters increasing the heat transfer at the gasket region. The presented methodology shows how to evaluate the gasket heat leakage with a combination of experimental and CFD results. Performing the experiment has some limitations due to the heat flux sensor applicability; therefore, a computational modeling was developed to calculate the total gasket heat leakages. A 2D cross section of the gasket region was designed and imported to "ANSYS FLUENT" to study the heat transfer across the gasket region computationally. The CFD provides a "shape profile" of the heat flux passing through the gasket region, but not the exact quantitative value of the flux. Thus, the calculated shape profile is used to be best fit the experimental data via the "Least Mean Square Error" method in order to provide a continues heat flux profiles over the gasket region. The profile is then numerically integrated to obtain the gasket heat leakage. This approach gives enough data to compare the gaskets and identify the most effective one.

In addition, a pure experimental methodology was developed to identify the air leakage, measure air exchange rate and its corresponding energy heat loss in the sample commercial refrigerator. Two separate refrigerators are used to get the air leakage measurements. These units are the same, but with different operating conditions. The first unit is a real unit which has a single obvious leakage path to the freezer, the water drain tube. However, as shown later, there are many additional leakages of unknown size and relative importance. The experiment with the real unit is used solely to measure normal operating conditions needed to mimic the conditions on the second unit. The second unit is an identical unit, but completely sealed with the drain tube open and a hole drilled in the wall of the fresh food compartment. The hole size is adjusted until the real pressure

differences between both freezer and fresh food compartments and ambient are achieved. This essentially recreates the operating conditions of the unsealed unit by providing an equivalent leakage area. Now the single inflow mass flow rate with a flow meter and the single mass flow rate out can be measured with both temperatures needed for finding the enthalpies. Having these data, the air infiltration rate and its corresponding energy loss can be calculated.

All experimental work reported was done by the author. All CFD results were done by his colleague, Mr. Feng Gao, and have been reported in a previous M.S. thesis [22].

2. GASKET HEAT LEAKAGE

Geometry complexity and heat leakage of the real refrigerator cabinet are the major reasons that made us come up with an idea to design and build a simplified cabinet concept, named the "Blue Box," for measuring the heat leakage through the gasket region (Figure 2.1 (b)). The main idea behind this approach is based on the energy conservation law. The blue box (Figure 2.1 (a)) contains a cubic interior volume of approximately 60 cm x 60 cm x 60 cm within which a heat load can be placed along with thermocouples to measure the enclosed air temperature. Adjoining refrigerator door and wall cut outs can then be placed inside the box so that the only portion exposed to the ambient environment is the gasket region, while thoroughly insulating all remaining sections with greater than 30 cm of insulation. The Blue Box operates by placing a heat source within the inner box, then bringing the entire mass to a thermal steady state. Both the (time averaged) interior and exterior temperatures are measured with thermocouples. Heat flux sensors are mounted on the outside of the exposed gasket region as shown in Figure 2.1 (b). Detailed CFD simulations are then conducted to match the experimental conditions but using a 2D slice of the Blue Box with matching exposed gasket section. Being 2D the CFD is not meant to predict the actual heat transfer and temperatures found in the experiment. The CFD only provides a "shape profile" of the heat flux leaving the gasket region along the coordinate, s, defined in Figure 2.2, in which the experimental heat flux sensors are placed. This shape profile can then be matched by a Least Mean Square Error (LMSE) analysis to the experimental data that essentially fills in the missing information between the six heat flux sensors. The resulting profile can then be numerically integrated along the 31 cm surface line and then divided by the experimentally measured temperature difference to provide

the heat leakages. Note that the door sections are removable and any set of doors can be cut and placed within the Blue Box for measurements. In addition, all CFD reported herein is completely predictive and produced using "best practices" described below. No model constants, grid refinement, or anything was changed to better fit any experimental data.

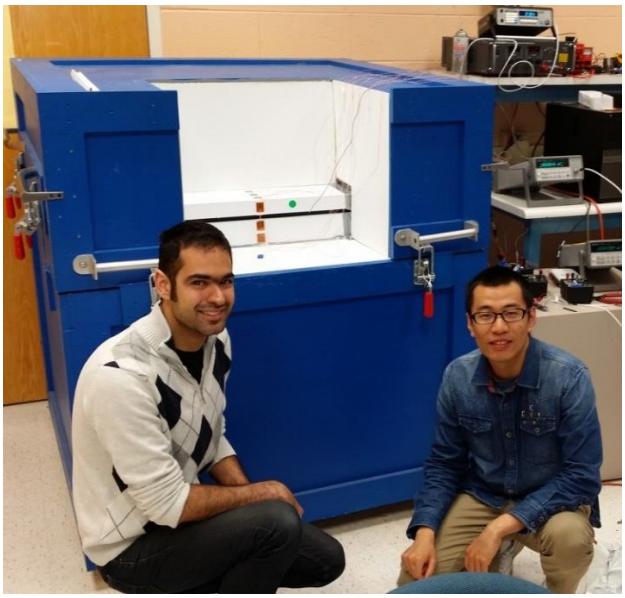

(a)

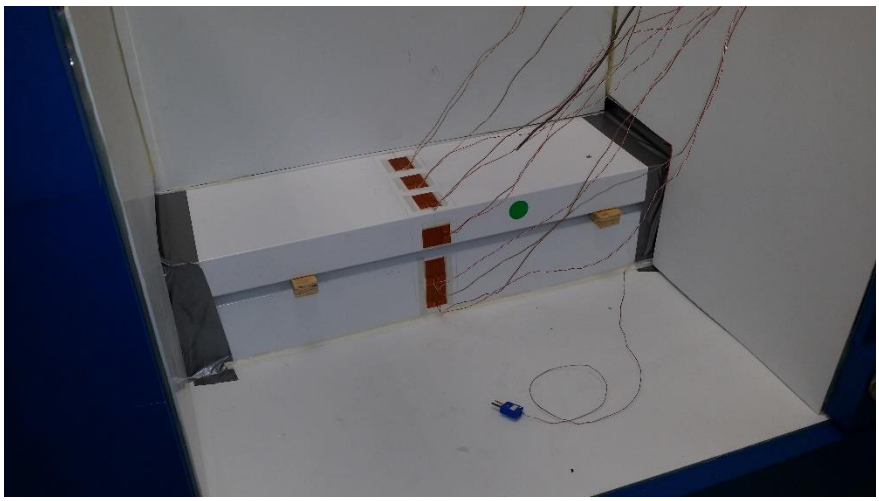

(b)

Figure 2.1: (a) Blue box, (b) picture of the six heat flux sensors positioned on the exposed portion of the gasket region

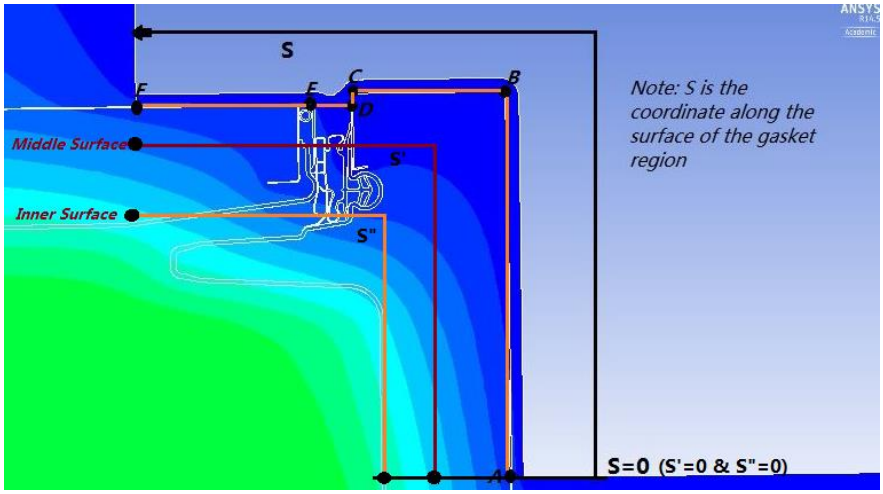

Figure 2.2: Temperature contours from CFD of a 2D cross section of the Blue Box

2.1. Gasket Region

The "gasket region" is defined as a 16 cm deep edge of the door section with a 15 cm section of the adjoining wall. The actual gasket itself occupies a 1.9 cm gap within the overall 31 cm long gasket region. However, the methodology developed herein allows the gasket region dimensions to be specified as any smaller portion of the exposed region that a user wishes to choose. The methodology developed allows for the determination of the gasket region heat leakage per unit time, per unit length and per unit temperature difference between the interior and exterior. Figure 2.3 shows the cross sections of the three gaskets which were investigated on this research.

Figure 2.3: Cross sections of the investigated gaskets

2.2. Test Facilities

Heat flux sensors and thermocouples with their associated amplifiers were used to measure temperature and heat flux values accurately. Also, some software filters are employed to reduce the noise of the signals to increase the measurement accuracy. A heater and a VARIAV were used to simply add the needed heat inside the box. The specification of the equipment used for running the test is discussed in this section.

2.2.1. Heat Flux Sensors

Heat flux, by definition, is a rate of energy transferred per unit time across a unit area. The unit of heat flux is watts per square meter ($\frac{W}{m^2}$) in the SI system.

$$q'' = \frac{q}{A} = -k\frac{\partial T}{\partial x} \tag{2.1}$$

A heat flux sensor is a transducer that converts the transferred heating energy to an electric signal which is proportional to the sensor thermal conductivity and the temperature difference existing across the sensor. A thermopile is a major component of a heat flux sensor. It measures the temperature using series connections of numerous thermocouples which gives the heat flux sensor the capability of getting the surface temperature difference across the HFS (Heat Flux Sensor). Figure 2.4 shows how heat flux sensor looks like.

Getting accurate heat flux measurements by heat flux sensors requires careful experimental design as well as implementation of calibration systems. Heat flux calibration is a procedure leading to mimic the measurement environment as close as possible with high repeatability. Diller [20] states that the presence of heat flux sensor may alter the temperature field causing error in results which can be reclined with an accurate calibration. Presence of air between the sensor and the attached surface can also cause some error in the measurement.

A variety of types of heat flux sensors are available based on application limitations. According to our application, a high sensitive heat flux sensor with capability of installation on curved and flat surfaces is required which makes it possible to measure low heat flux values and generate measurable output voltage. After a careful investigation on calibrated heat flux sensors, HFS-4-Omega is chosen in order to measure heat flux for our application. Low thermal impedance, high sensitivity, fast response, wide temperature operation and flexible surface are the highlighted features for the specified heat flux sensor. It is a self-generating device requiring no external voltage or current stimulation so that the sensor does not generate any additional heat itself. However, being self-generating causes the sensor output voltage to be very small which makes the calibration procedure

complicated. The sensor sensitivity is $6.5\frac{\mu V}{\frac{Btu}{Ft^2-Hr}}$; therefore, heat flux variations are not detectable by a DAQ system with 16 bits resolution. However, any commercial amplifier with microvolt resolution can boost the sensor signals to a higher level which is readable by the DAQ system. Note that the output of the selected amplifier is specified based on the resolution of the data acquisition system.

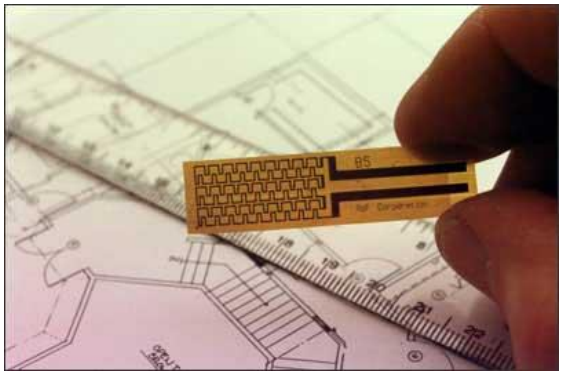

Figure 2.4 Heat Flux Sensor

To mount a heat flux sensor, the following should be considered:

- An appropriate adhesive tape should be used for sticking the sensor on the surface. The temp-rating for the adhesive tape should be higher than 200°F.
- The heat flux sensor should be securely mounted on the surface with no air bubbles or gaps. Presence of air between the sensor and surface leads to an error in measurements.

- The heat flux sensor should be mounted in the right direction. Positive (+) values for heat flux must refer to the heat that is going into the surface that the sensor is mounted on; likewise, negative (–) for heat flowing out of the surface.

2.2.2. Amplifier (Nano-Voltmeter)

Heat flux sensors are extremely sensitive devices requiring a suitable amplifier to measure their low output signals, as low as $10^{-3}\ \mu V$, and amplify them to an appropriate level which is proper for the DAQ system input. All these heat flux sensors should be directly wired to the nano-voltmeter (or a sufficient amplifier) so that their generated output voltage can be measured. The nano-voltmeter is required because the output from the heat flux sensors is at the micro-volt level. The nano-voltmeter has an internal signal conditioner which has a primary use of converting a signal that is difficult to be read by the data acquisition into a more easily read format.

According to the requirements, Agilent 34420-A is the preferred amplifier for our application. Agilent 34420-A is basically a nano volt meter with low noise and high-gain technology of measurement. It can measure a large voltage interval between 10nV to 1000 V based on the application. The resolution of this nano voltmeter is 10^{-8} V which works best for getting voltage measurement from the heat flux sensors with μV range output. It benefits from analog output letting the nano voltmeter communicate with the DAQ system to transfer the displayed readings to the computer. The nano-voltmeter has two input channels and one analog output; therefore, at each stage of the experiment, two heat flux sensors can be connected to the nano-voltmeter, but just one of their responses is reported

to the data acquisition system at a time. Accordingly, after recording the response of one of heat flux sensors, it is necessary to switch the heat flux sensor manually and measure another response. There were two nano-voltmeters on hand for the experiments; therefore, two measurements at a time were taken.

A suitable gain for the nano-voltmeter is defined regarding the input and the desired output. The output voltage is related to the input signal as follows:

$$\frac{Reading}{Span} = Chart\ output\ Voltage \tag{2.2}$$

2.2.3. Thermocouple

A thermocouple is widely used for taking temperature measurements. It is operating by converting a temperature gradient into electric signals. Thermocouples are available in a variety of "types" such as K, T, N, J, etc. A proper thermocouple type is selected by considering the working temperature interval and the atmosphere conditions. T type working temperature interval is ranged from −250℃ to +400℃ which meets our application requirements. This type of thermocouple is self-powered, so it requires no external power to generate electrical signals. Two different kinds of T type thermocouples are measuring the temperature variation in our application. The first model is an insulated thermocouple measuring the interior and exterior air temperature for the experiments. It is also used to determine and specify the thermal boundary layer to substitute the values into CFD simulations. The thermal boundary layer has a great impact on CFD calculation since significant temperature variations occur in this specific layer. The second model is an

adhesive T type thermocouple which is suitable for any flat surface temperature measurement. It is simply fixed on any flat surface in order to measure its temperature.

Wide range operation, fast response, high precision and signal stability are the advantages of employing thermocouples for measuring the temperature [21]. They are also rugged transducers which are insensitive to vibration and capable of being used in hazardous environment. However, note that, achieving system errors of less than one degree Celsius (°C) is the limitation of using thermocouple for getting temperature measurements. The thermocouple output signal is in the range of microvolts so that a few microvolts of noise pick up can result in significant errors in temperature measurements. Therefore, there are some hardware and software features recommended to restrict any possible noises.

2.2.4. Thermocouple Amplifier

Amplifying signals is a process of manipulating the input signals in such a way that makes the input signals suitable to be read in the next stage for further processing. The thermocouple output signal is less than 75 millivolts and most of the data acquisition systems are not sensitive enough to be driven directly by that small signals. Therefore, an amplifier is connected to the thermocouple to boost the signals. It is recommended to try using lower gain settings first and use no greater gain settings than is required.

2.2.5. Anti-Alias Pre-Filter

Anti-alias pre-filter is a function to reduce the high-frequency noise compartment in the analog signal coming from the sensor. It is placed between the A/D (analog to digital) convertor and the sensor to prevent aliasing. It is worth it to mention that aliasing occurs when the sample rate is not at least two times higher than sample frequency.

2.2.6. Low Pass Filter

A low pass filter, by definition, is a filter that can pass signals with frequencies lower than the specified cutoff frequency and attenuate signals with frequencies higher than the defined cutoff frequency.

2.2.7. Poor Junction Connection

The thermocouple wires eventually break after lots of usage so it is recommended to connect the bare wires to a connector to protect wires from being damaged. Connectors are in different types, it is necessary to use a connector with the same type of the connected thermocouple.

2.2.8. Calibration

Calibration is one of the most complex procedures of setting up the experiments. The thermocouple temperature-voltage relationship is nonlinear. Note that any decalibration can result in a temperature reading which appears to be correct. Accordingly, enough attention should be paid to apply the calibration curve to the output signals.

2.2.9. Sample Compression

Sample compression is a function that acquires a large number of data points and takes their average which results in reducing them to a single data point in the resultant signal. The amount of the acquired data is specified by reduction specification.

2.2.10. Data Acquisition System

A Data Acquisition System (DAQ) is utilized to process the electrical signals which are being fed via connected sensor or transducers like pressure transducer, heat flux sensor, thermocouple, etc. The processed electrical signals are proportional to the quantity of the physical phenomena being measured. The DAQ system is able to print out the measured signals via a USB cable to a desktop computer. The data can be primarily monitored on the computer by a software package like LabVIEW or any equivalent software package. Then, raw data are converted to physical units and stored on the computer. Number of I/O Channels, maximum sample rate, portability, software Compatibility, operating System, bus and resolution are the factors which should be considered in selecting a proper data acquisition system for any applications.

2.2.11. Current Sensor

Current sensors can detect and measure AC or DC electrical current and generate an output voltage proportional to the measured current. This kind of sensors is provided with wide varieties of input and output ranges. Input current interval and output signal range are the factors that should be considered to select an appropriate current sensor for any application.

2.3. Experimental Setup

This research is mainly focused on the experimental portion of the study. The author has provided some assistance with the CFD simulations [22]; however, his contribution and the content of this thesis are predominantly on the experimental portion. Figure 2.5 shows the flow chart diagram of the sequence of experimental procedure for measuring, recording and displaying the temperature and heat flux values from the blue box.

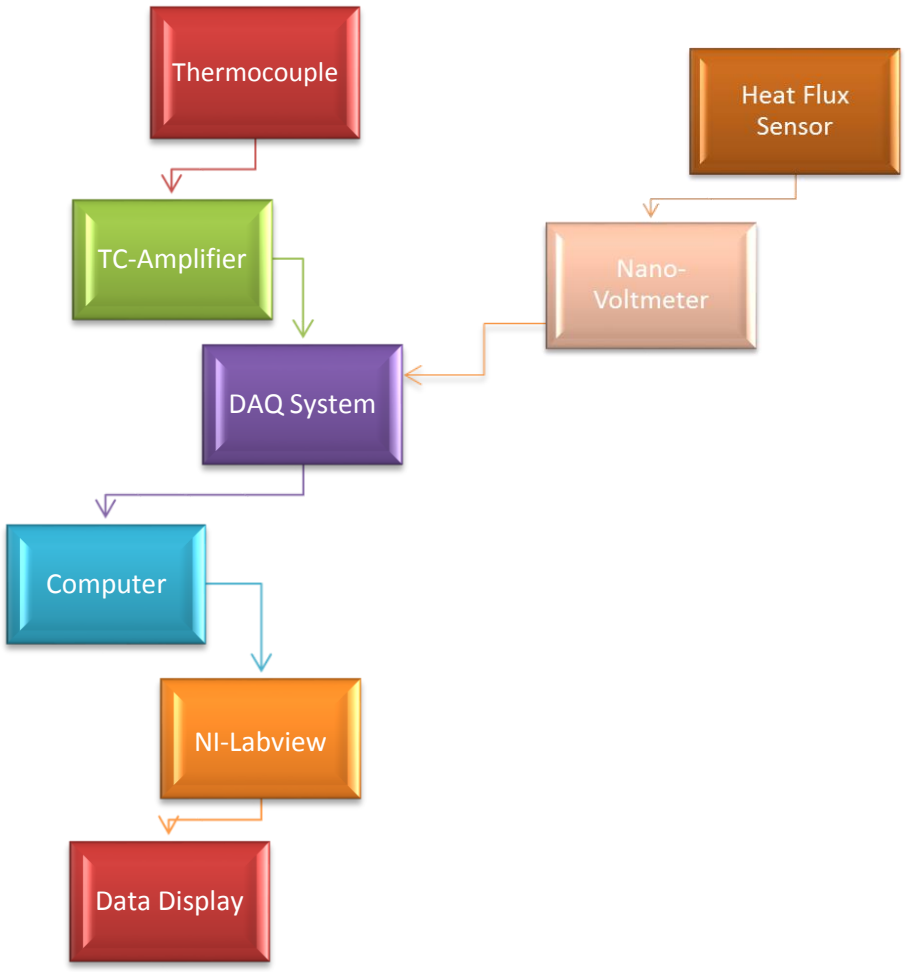

Figure 2.5: Flowchart for hardware connections

The Reverse Heat Load experiment is mainly falling into two separate parts; one is generating a temperature difference and the other measuring the heat leaking through the gasket region. Heater, power supplier, voltmeter, and ammeter are the required equipment to warm the interior and quantify the input power. On the other hand, heat flux sensors, thermocouples, TC amplifier, nano-voltmeter (or capable amplifier), data acquisition system, desktop computer, and a software package (LABVIEW or equivalent) are required in order to measure heat leakage and temperature differences as well as process and store the data.

A heater is placed inside the box to produce a desired temperature difference (Figure 2.6). The heater is directly wired to a power supplier placed out of the box. The power supplier has an indicator which shows how many volts it is supplying to the heater. If the indicator is not very accurate, a voltmeter can be connected to the power supplier in a parallel circuit for measuring the output voltage of the supplier. An ammeter must be connected to the power supplier in a series circuit to measure the electric current. The power applied to the heater is simply calculated from voltage value times current value, $P = V \times I$.

The rate of energy leakage from the gasket region must be measured. This is the most sensitive part of the experiment since any small changes in each of the factors has a significant effect on the final results. The heat flux sensors are very sensitive and must be carefully, and well, adhered to the surface. To equip the box with the measurement equipment, first start with the thermocouples. We mounted at three thermocouples to measure the air temperature in the lower, middle, and upper elevations within the box. Another thermocouple is required to be placed out of the box to measure the ambient

temperature. All these sensors should be directly wired to their associated TC amplifiers. The TC amplifier has different gains to set on; however, note that it is recommended to try using lower gain settings first and to use no greater gain settings than required to minimize signal noise. As far as we have investigated, 25 is the best value for the gain to be set on the amplifier based on range of the temperature measurement in our application. Finally, all the TC amplifiers and nano-voltmeter should be wired to the data acquisition system. The function of data acquisition system is to process all these signals and transfer them to a computer to be recorded and analyzed. The computer needs a software package such as LabVIEW to convert these signals to desired temperature or heat flux units. Calibration curves are provided by the manufacturer for all sensors. All wiring was run through two holes drilled through the side of the box (one for the power cable and another for the sensor wiring). Insulating silicone was then applied to fill the holes.

For the present experiments, six heat flux sensors are required to be placed on the exposed gasket region (Figure 2.1(b)). The corresponding locations of the six heat flux sensors used in the experiment are at s locations: 0.03m, 0.09m, 0.14m, 0.192m, 0.258m, and 0.303 meters (Figure 2.1(b)). These heat flux sensors are very sensitive to air motions in the room. The data they generate oscillates widely when disturbances to the room occur; including the AC turning on, doors opening, even people walking nearby. Therefore, a protective plastic sheet was taped over the sensor section for all data collection (Figure 2.7) This, and sufficient time averaging of data, proved sufficient for the purposes of this study. Note though that when measuring the “ambient” temperature needed for the temperature difference across the gasket region, the outside thermocouple(s) is placed within the covering.

Figure 2.6: A view inside of the instrumented Blue Box (for experiments the heating element is centered within the box)

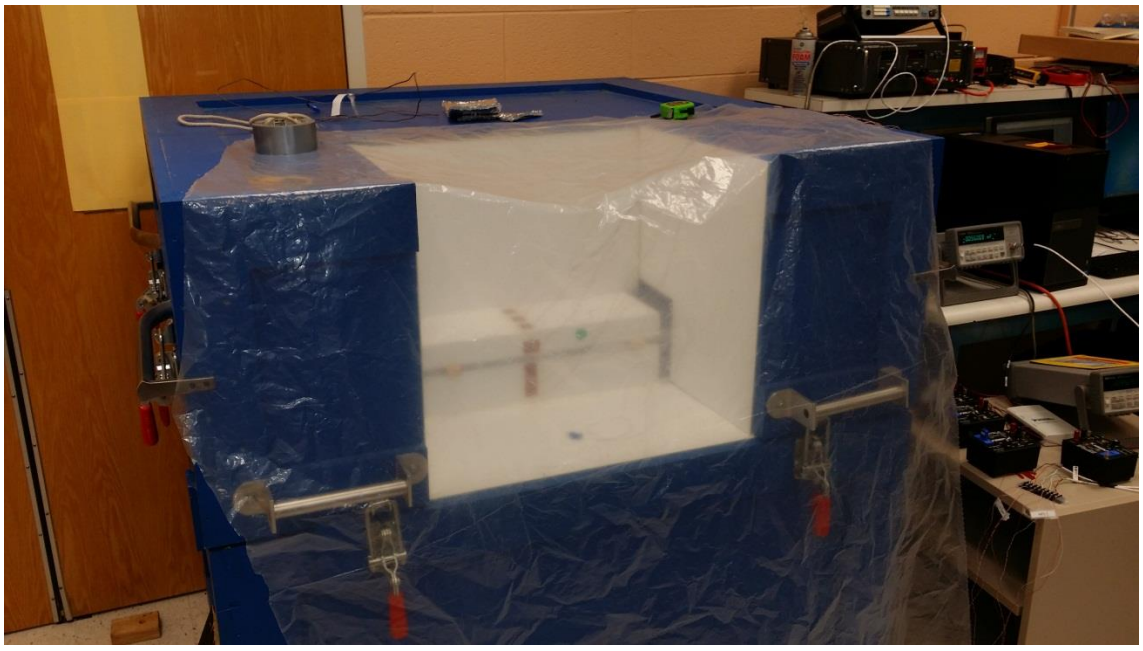

Figure 2.7: protective covering to minimize heat flux sensor noise due to air motion. This was later cut to fit better and taped along the edges with duct tape

Once sealed, the Blue Box still has several locations that require additional insulation in the form of added silicone on top of duct tape (so it can be removed easily). A thermal imaging camera proved useful in locating gaps needing additional insulation (Figure 2.8).

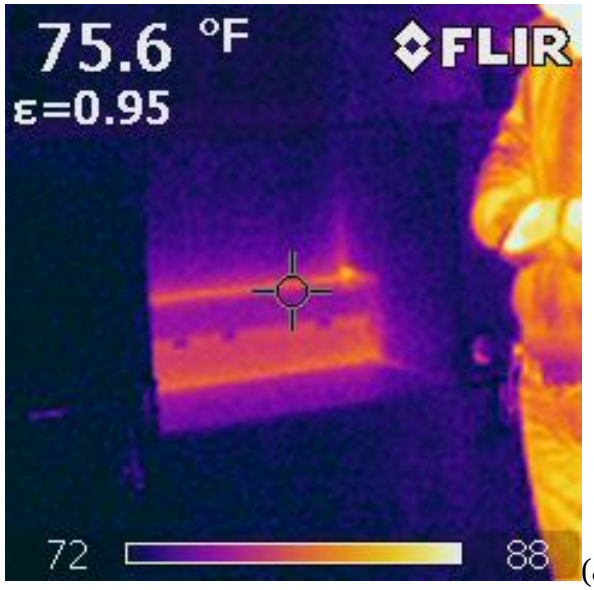

(a)

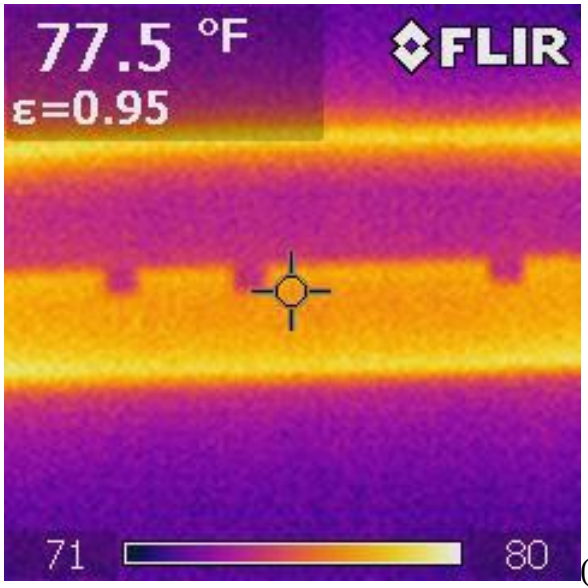

(b)

Figure 2.8: Thermal camera images of the Blue Box: (a) from approximately 3 m away with one of the students in the picture for perspective, and (b) a close up of the gasket region

It is also crucial to use a fiberglass adhesive tape with sufficient temperature rating to mount the sensors inside the box so that the sensors will be tightly stuck to the wall during the experiments. To mount the heat flux sensor, it is very important to visually inspect each sensor to ensure it is securely mounted to the surface with no air bubbles or gaps. Any such defect was found to result in large amounts of noise in the signal and erroneous heat flux values. Therefore, the sensors should be mounted as tightly as possible to the wall and adhesive tape should cover all exposed edges. Note that the heat flux sensors come with their own adhesive coating. We chose not to use it though as the sensor can only be moved once or twice this way.

To start reading the data points from the sensors, the box should first reach a steady state condition after the heating element is turned on, the box is sealed, and all additional silicone and tape insulation is added. From a "cold" start, it is found that it takes approximately three days to reach the steady state condition. When simply opening the box to make changes relatively quickly the box remains "hot" and typically one day is sufficient to get back to steady state. Some steps should be taken to confirm that the box has reached the steady state condition. First of all, start recording the primary data points and keep waiting till the inner air temperature does not change significantly (see Figure 2.9).

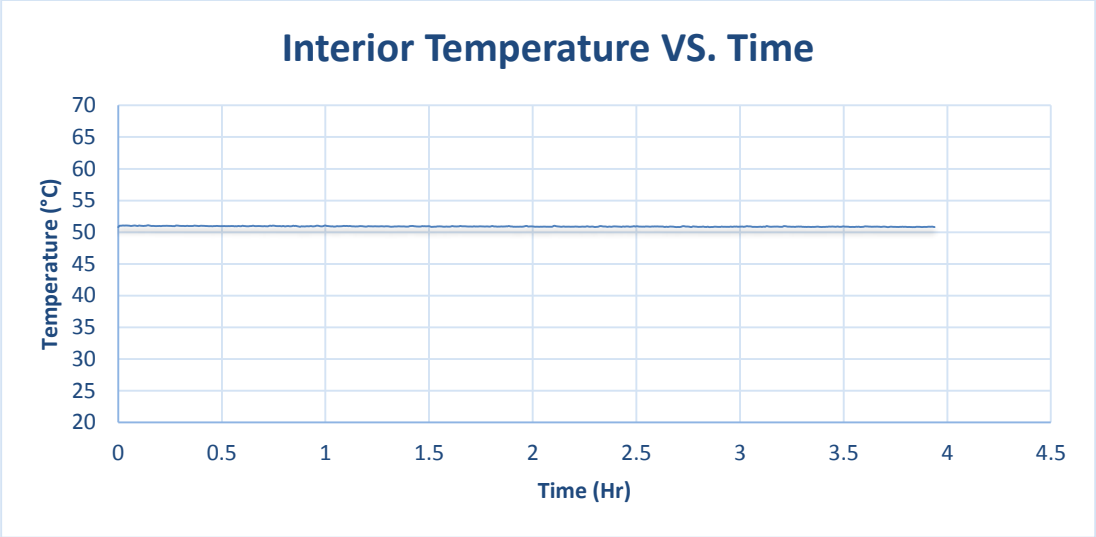

Figure 2.9: The inner air temperature vs. time from Experiment #3 at steady state

Next, the running averaged temperature is calculated as a function of time to determine how long averaging must be done to achieve converged experimental values (Figure 2.10). The same procedure is done for the heat flux sensors. To quantify the deviation from the average values, the next step is calculating the standard deviation from all data points after determining the average. Figure 2.10 illustrates a running calculation of the standard deviation of a temperature signal. The standard deviation, or root mean square (rms), provides a measure of how much the signal oscillates about its mean. Approximately four hours is needed to fully collect converged statistics.

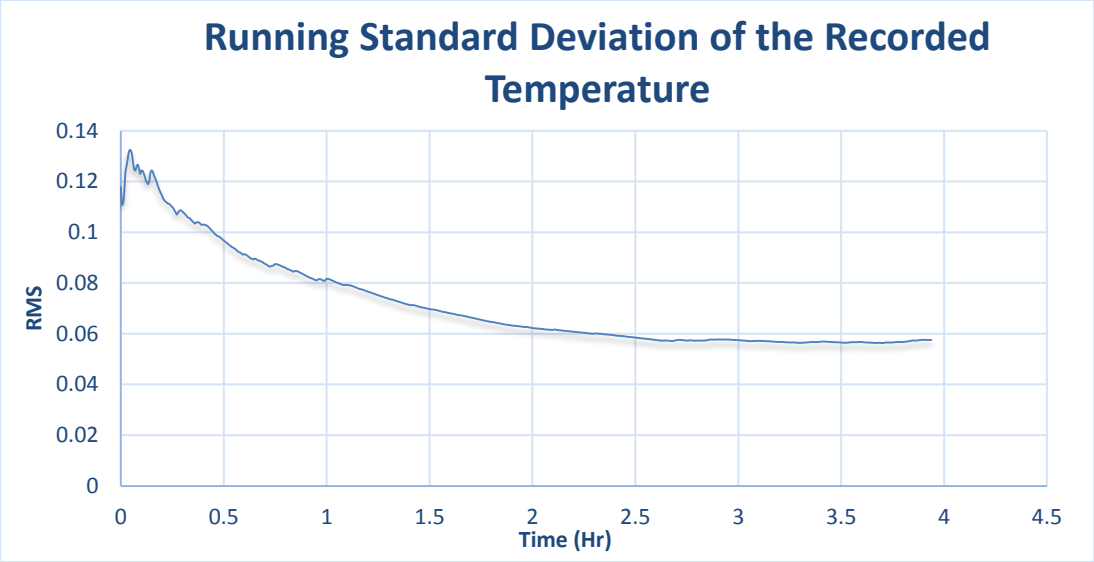

Figure 2.10: The running standard deviation of the temperature signal associated with Figure 2.9

The heat flux sensor signals are treated in a similar manner. Both running average and standard deviations of heat flux data are calculated for all. Figure 2.11, Figure 2.12, Figure 2.13 illustrate a typical (steady state) heat flux sensor instantaneous reading, running average, and running standard deviation, respectively.

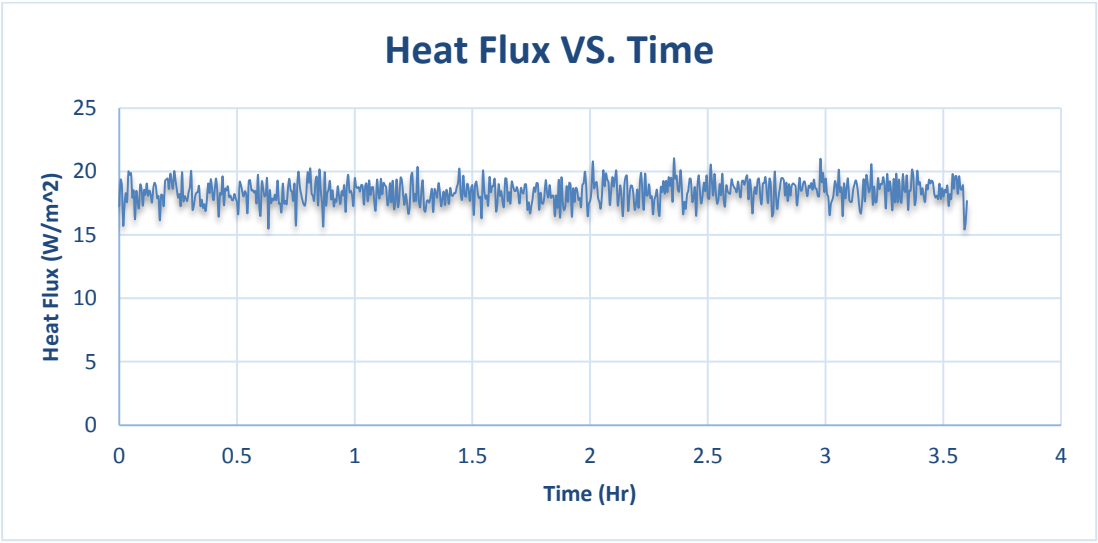

Figure 2.11: Example instantaneous heat flux sensor reading as a function of time

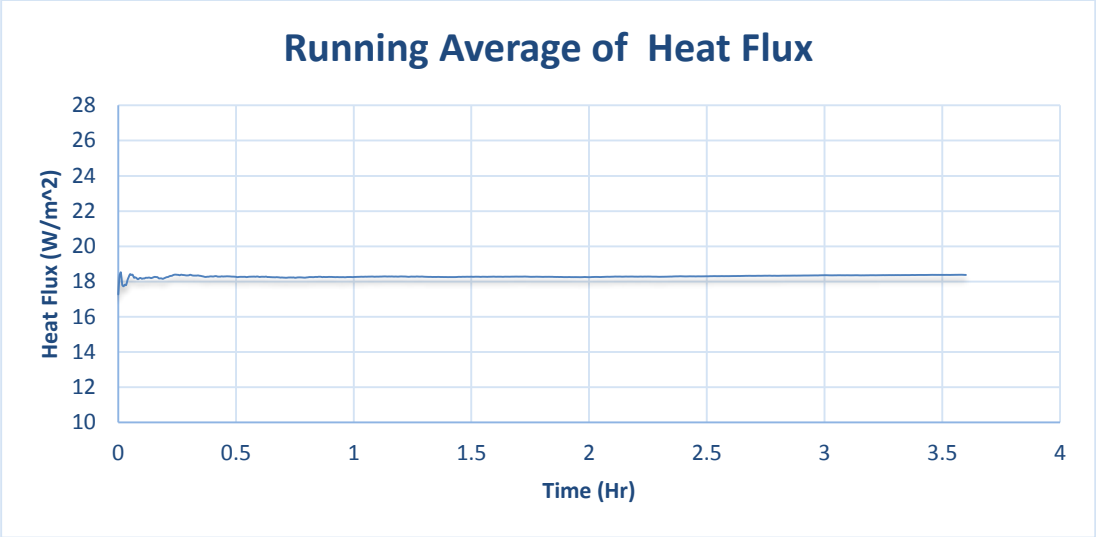

Figure 2.12: Example running average heat flux sensor reading as a function of time

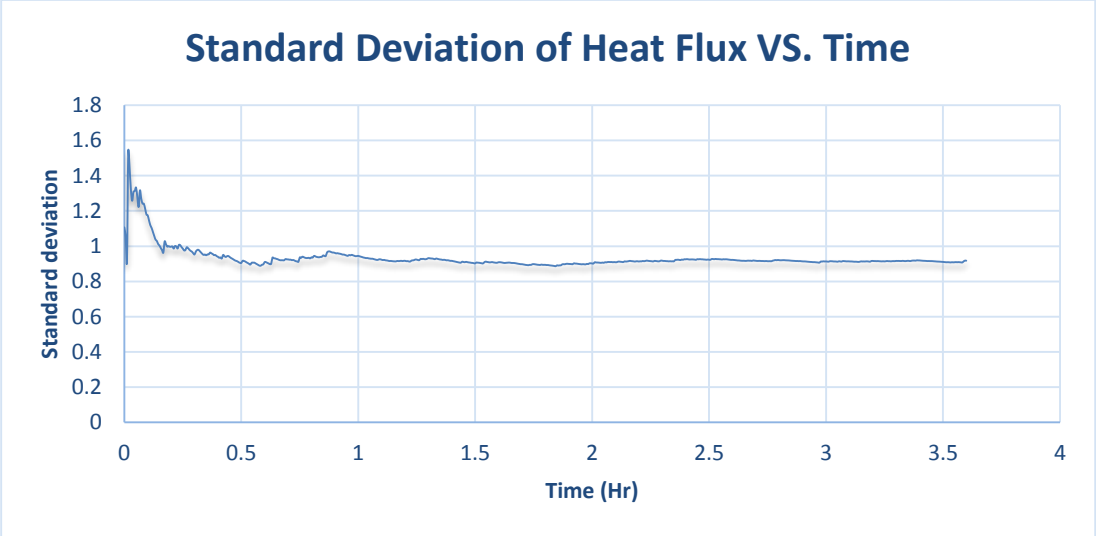

Figure 2.13: Example running standard deviation heat flux sensor reading as a function of time

All sensors were sampled at a rate of 0.5 Hz. This provides a very sufficient time resolution of all signals while maintaining reasonable data file sizes for post processing of the averages and standard deviations. Final averages and standard deviations from all six heat flux sensors from all five experiments are provided in Appendix A.

2.4. Experimental Results

Temperature and heat flux measurements for three different gasket models with three different input loads are presented. The repeatability of the heat flux measurements were also investigated and reported in this section.

2.4.1. Temperature Measurements

The test was run for three different gasket models with three input heat loads. The first set of experiments were conducted with a single gasket but different heat loads in order to find out the temperature differences created across the gasket associated with the specified input powers. Therefore, 9.2, 13.14 and 18.13 watts were set on the heater, resectively, and their associated temperature differences were recorded. Table 2.1 presents the final teperature difference created across the first gasket, named “original”, after reaching the steady state conditions with repect to the input heat load powers.

Table 2.1: Recorded temperature difference for three different heat loads with a single gasket

Exp.	Gasket	Heat Load	ΔT
1	1, original	9.2 W	20.2 K
2		13.14 W	26.6 K
3		18.13 W	34.6 K

Afterward, two more gasket were installed on Blue box while a single heat load, 13.14 watts, was adjusted on the heating element. The temperature difference appeared on the final temperatures existing across the gasket can simply illustrates which gasket is the

more effective compared to the other investigated gaskets. Table 2.2 shows the final temperature differences created across different gaskets.

Table 2.2: Recorded temperature difference for three different gaskets with a single heat load

Exp.	Gasket	Heat Load	ΔT
2	1, Original	13.14 W	26.6 K
4	2, Black Side-by-Side	13.14 W	25.2 K
5	3, White	13.14 W	25.6 K

2.4.2. Heat Flux Measurement

Based on the aforementioned, six heat flux sensors are placed on the exterior surface of the exposed gasket region (Figure 2.1(b)). Table 2.3 shows an example of the heat flux reading values from mounted heat flux sensors at their certain locations. To review all the recorded data for the conducted experiments, please refer to Appendix A.

Table 2.3: Example of measured heat flux running through the exposed gasket region for the expriment#1, Original gasket, $\Delta T = 20.2℃$, $\Delta T_{rms} = 0.148℃$

Sensor	*Mean* ***Heat Flux*** $(^{W}/_{m^2})$	*RMS* ***Heat Flux*** $(^{W}/_{m^2})$
HFS 1	17.3	1.94
HFS 2	12.2	1.55
HFS 3	4.76	1.06
HFS 4	8.57	0.71
HFS 5	19.7	1.31
HFS 6	20.5	0.6

2.4.3. Repeatability

Repeatability of the experiments was also thoroughly investigated. Several of the experiments were repeated with more than a week between runs. Figure 2.14 provides an example of two such data sets that were obtained for the conditions of the experiment with the white gasket (Experiment #5). Data are shown from two different runs of the same experiment performed, demonstrating the reproducibility of the results. The "error" bars are the standard deviation of the data used to calculate the average heat fluxes

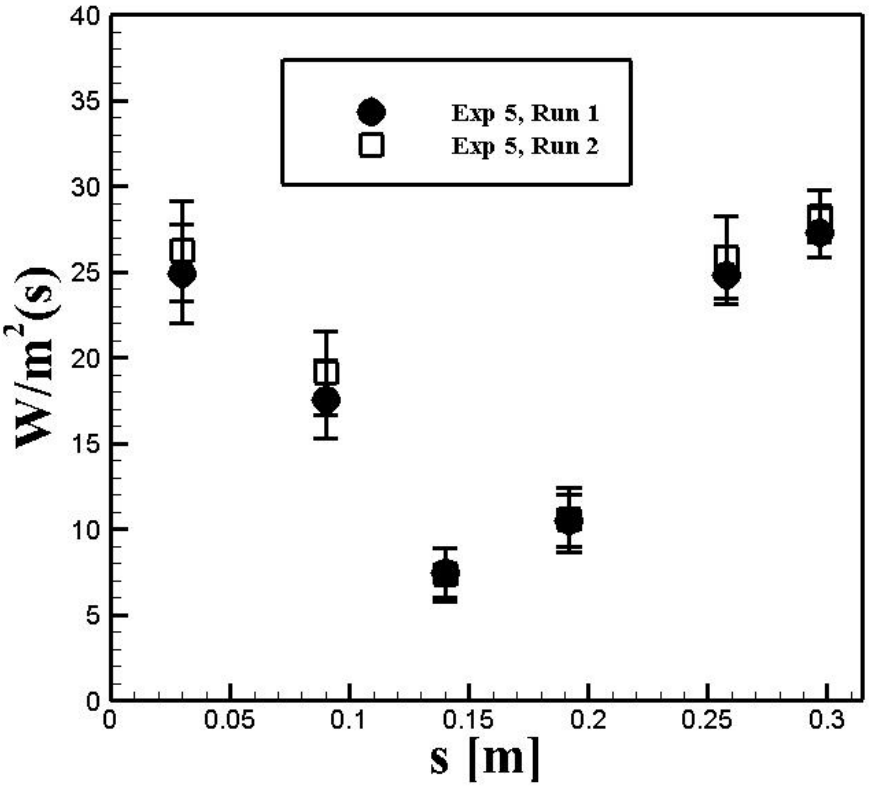

Figure 2.14: Measured surface heat flux distribution as a function of the surface path s for Experiment #5

2.5. CFD Simulation

CFD simulation is performed based on the exact dimension of the Blue Box but in a 2D cross section; 3D simulations being extremely computationally taxing and not necessary for present purposes. For learning more about the performed CFD simulation procedure, please refer to Mr. Feng Gao master's thesis "Numerical simulation of the heat leakage at the gasket region of domestic refrigerator" [22]. As discussed above, the purpose of the CFD for this investigation is only to produce heat flux surface "shape factors." Being 2D, the CFD is not expected to produce the actual experimentally measured surface heat fluxes or temperature differences. However, the "shape" of the gasket surface heat flux profile should be extremely similar to that of the experiments conducted along the center plane of the Blue Box. The assumption is that the shape factors produced by the CFD can then be scaled to "best fit" the experimental data to provide the entire surface heat flux distribution. For present purposes, "best fit" is defined as the scaling of the CFD produced surface profiles that minimizes the square error of the CFD profile with the six experimental heat flux sensor measurements for each configuration of the experiment. This is the "Least Mean Square Error," or LMSE, approach to error minimization. The FORTRAN code used to evaluate the LMSE for Experiment #1 is provided in Appendix B. This assumption that the CFD produced profiles will match the shape of the real 3D surface heat flux distribution is confirmed in the following. Note that several CFD simulations were implemented based on the applied heating powers and gasket geometries used for conducting the experiments.

As shown in Figure 2.15, the simulations are based on the 2D geometry of the blue box (cross-section). The orange rectangle in the following picture represents the heating element. The power of this heater is specified based on the experimental specifications. Figure 2.16 shows a zoom in of the gasket region for original gasket. Note that a 5 mm thick portion of the ambient air along the gasket region is included in the domain. The first step in conducting a CFD simulation in Fluent (or any CFD package) is specifying the geometry. This can be either internally in the ANSYS package through their Design Modeler software, or externally through a variety of packages such as CATIA or SolidWorks, then imported back into ANSYS.

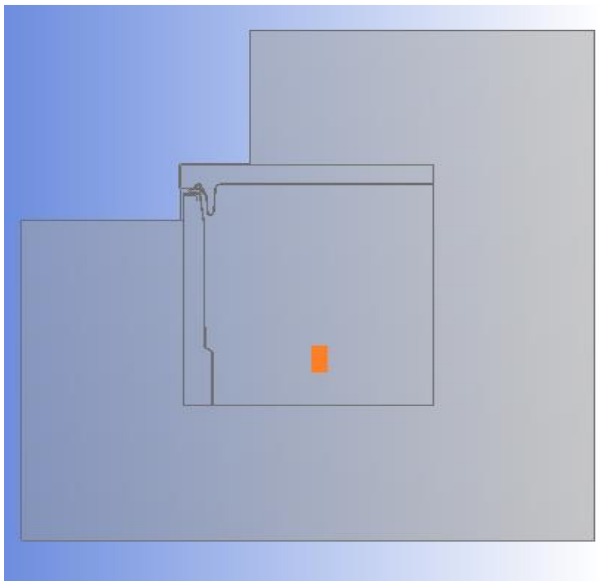

Figure 2.15: The 2D geometry of the blue box used in CFD simulation. The gravity vector points to the left of the figure

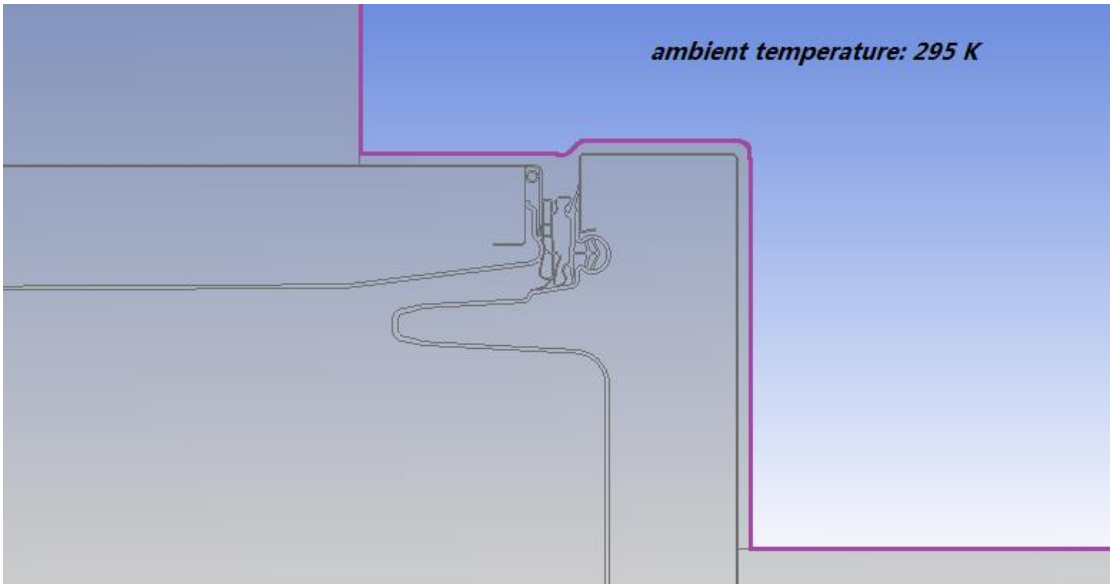

Figure 2.16: Zoom in of the (a) gasket region of the domain and specification of the boundary condition implemented in the CFD simulations

The exact geometry of the all the investigated gaskets were perfectly designed and imported to ANSYS fluent to provide a specific heat flux shape profile for each gasket.

2.6. Combined Experimental and Computational Methodology: Final Product

Figure 2.17 shows all of the "raw" data obtained from the experiments and the CFD of the Blue Box. There is a final step in the process for the data of Figure 2.17.

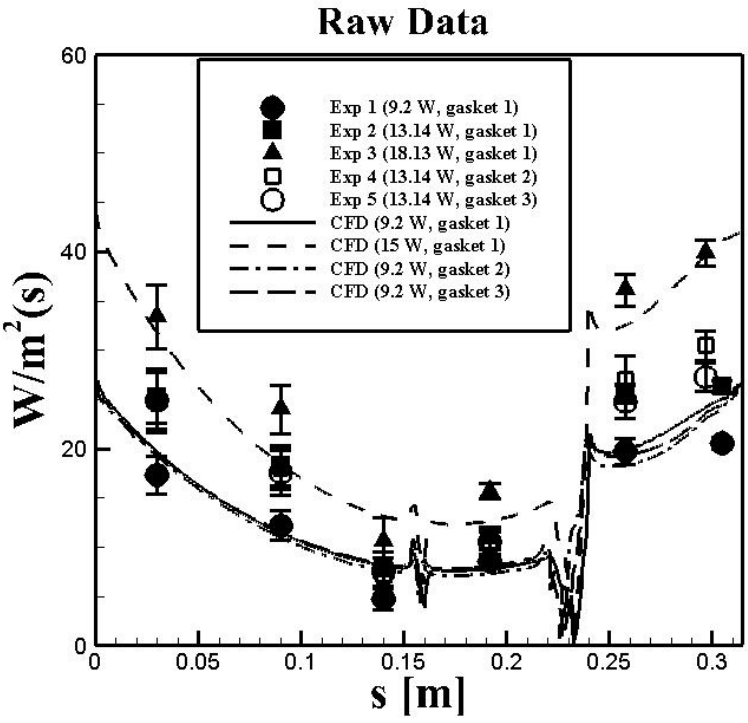

Figure 2.17: Experimental and CFD obtained surface heat fluxes as a function of the surface path coordinate: the original "raw" data

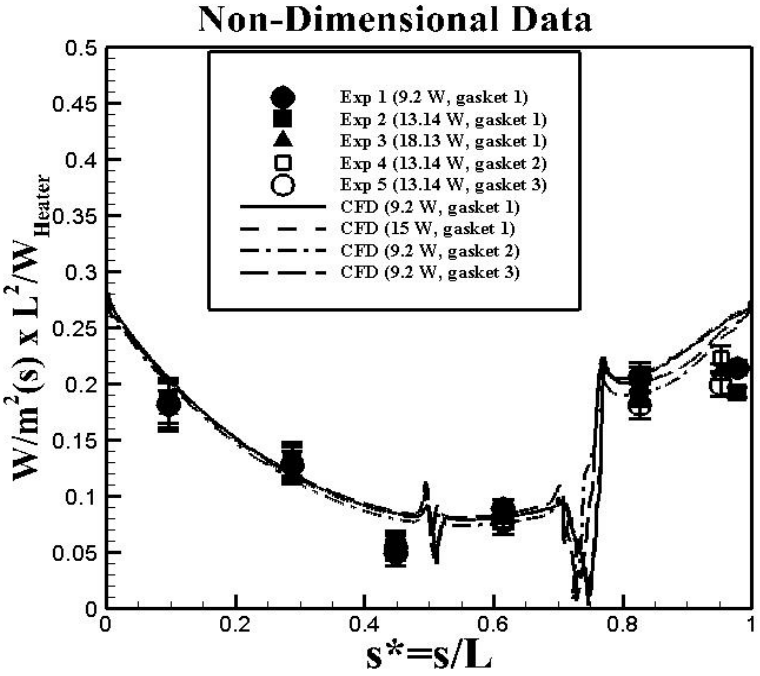

Figure 2.18: the same data non-dimensionalized by the surface length and the heat load in Watts. The "error" bars are the standard deviation of the data used to calculate the average heat fluxes

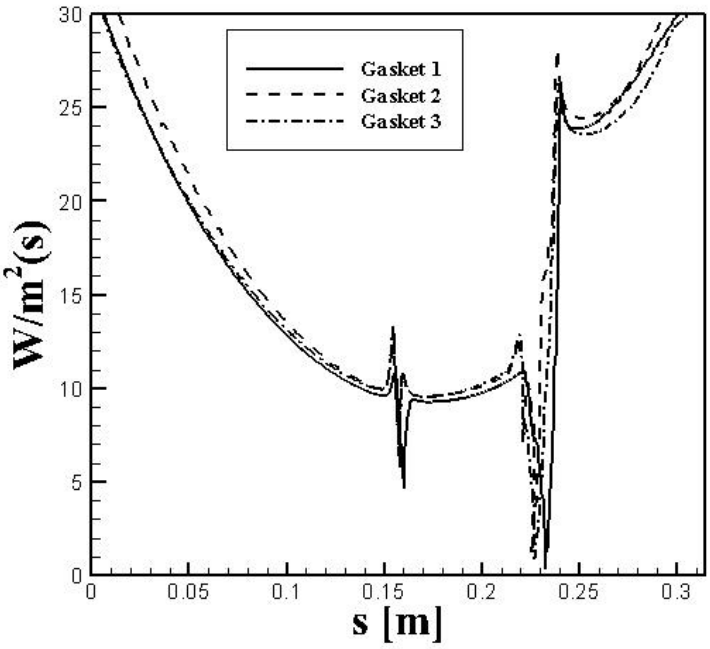

Figure 2.19: Comparison of the surface heat flux profiles for each of the three gaskets with a 13.14 W heat load (Experiments 2, 4, and 5)

As stated above, the CFD is 2D and is not expected to produce the same temperature differences as the 3D Blue Box (in the CFD the heating element is infinitely long in the third direction). Nevertheless, the "shape" of the surface heat flux is expected to be the same in the 2D CFD in comparison to the centerline (symmetry plane) of the Blue Box surface. Therefore, the CFD is only used to produce the shape factors necessary to fill in the information between the six experimental heat flux sensors. What needs to be determined is the multiplication factor needed to correct the CFD produced shape factors to "best fit" the experimental data. Note that for a given gasket any of the CFD profiles produced at the various heat loads can be used as the profiles are independent of temperature difference when normalized (Figure 2.18). The "best fit" is defined for present purposes as that scaling factor which minimizes the mean square error – the so called Least Mean Square Error (LMSE) approach.

This process occurs as follows. First, a CFD shape profile is chosen for the particular gasket (eg. 9.2 W for Experiment #1). Next, the six CFD calculated values of the surface heat flux corresponding to the locations of the six heat flux sensors used in the experiment are extracted; ie. at s= 0.03 m, 0.09 m, 0.14 m, 0.192 m, 0.258 m, and 0.303 m (Figure 2.1(b), Figure 2.2). We then want to find the scaling parameter, α, that, when multiplying the six CFD values, minimizes the mean square error with the six experimental data points. The mean square error is defined as:

$$MSE = \frac{1}{N}\sum_{i=1}^{6}(\mathrm{Expi} - \alpha\ \mathrm{CFDi})^2 \qquad (2.3)$$

In practice this is done using a short code written in FORTRAN that cycles through values of α in small increments over a reasonable range and then reports the value that produced the minimum error. An example code is provided in Appendix B.

Once obtained the entire CFD curve for that experiment is multiplied by the correction factor α and the experimental data and corrected CFD profile can be plotted and/or analyzed (e.g. Figure 2.20, Figure 2.21).

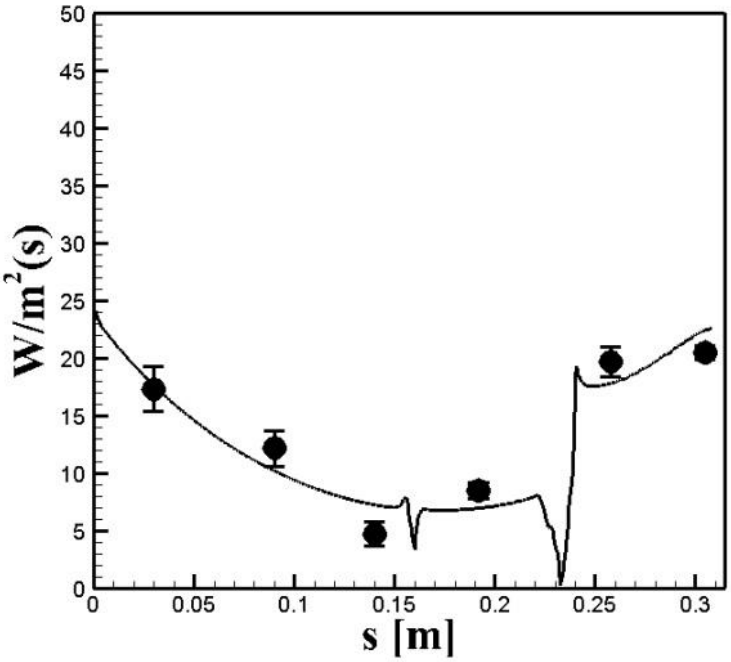

(a)

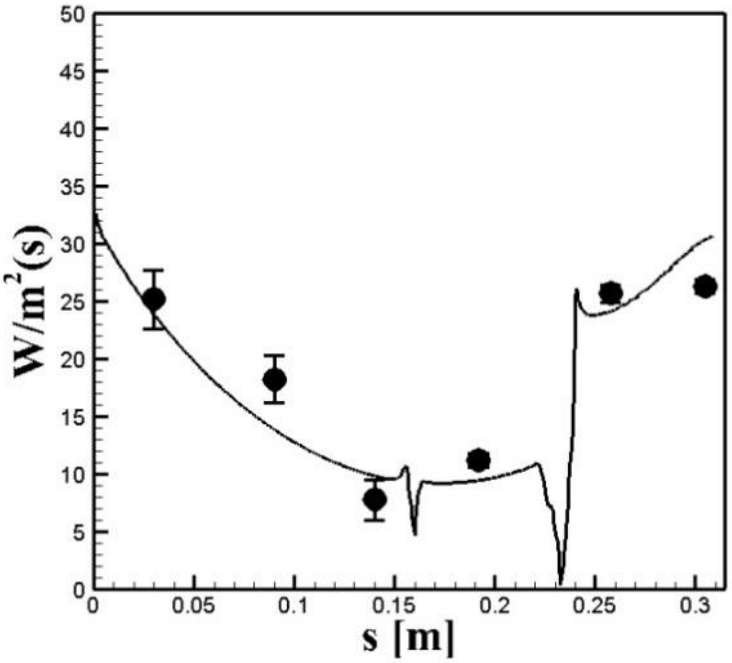

(b)

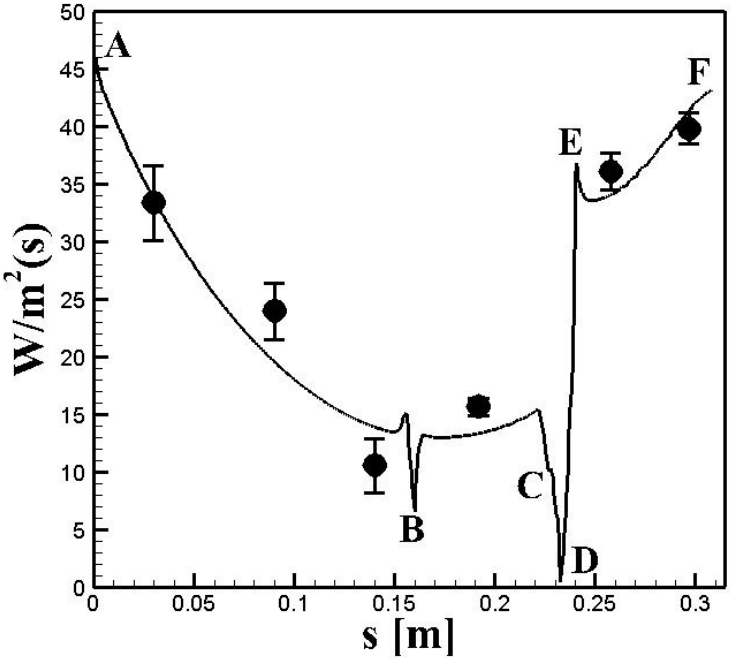

(c)

Figure 2.20: Best fit (Least Mean Square Error) surface heat flux profiles for Experiments (a) #1, (b) #2, and (c) #3 – varying heat loads all with the originally supplied gasket. The "error" bars are the standard deviation of the data used to calculate the average heat fluxes. Part (c) also labels the locations A-F corresponding to those of Figure 2.1 (b).

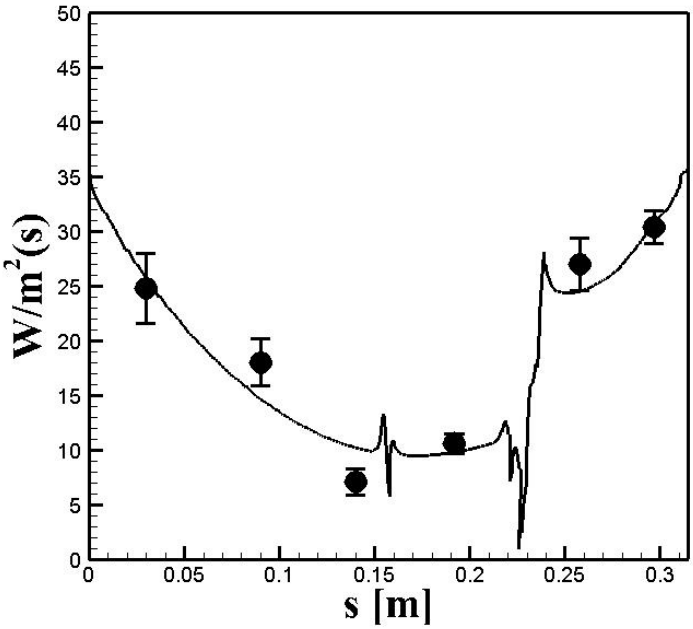

(a)

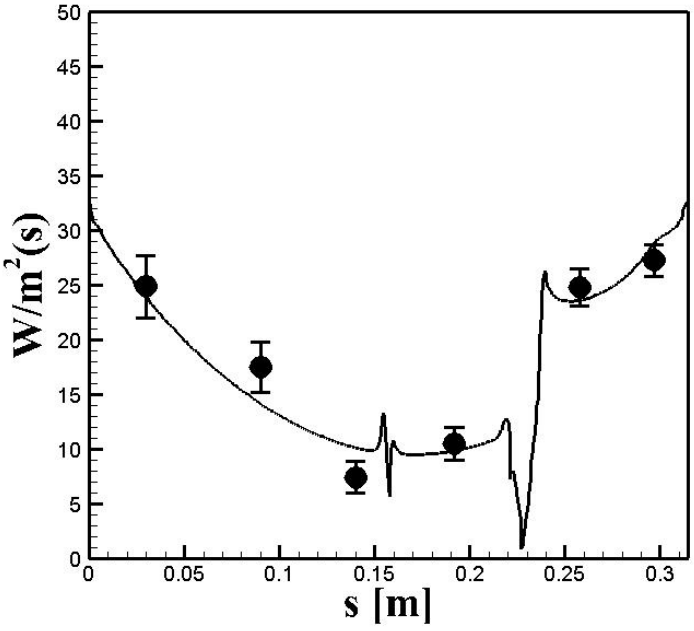

(b)

Figure 2.21: Best fit (Least Mean Square Error) surface heat flux profiles for Experiments (a) #4 (black side-by-side gasket), (b) #5 (white gasket), at fixed heat load. The "error" bars are the standard deviation of the data used to calculate the average heat fluxes.

The final CFD profile is then numerically integrated over the entire domain length for the path "s" of Figure 2.2. This yields the heat leakage rate in Watts per unit length of the gasket region, W/m. We use a commercial plotting package, Tecplot, to produce most of the plots in this report. It has a numerical integration tool built in that was used to obtain the W/m values reported herein. However, a similar FORTRAN (or other language) code could easily be written to perform the numerical integration. Note too that any domain length can be chosen if one wants to define the "gasket region" as something smaller than the 31 cm wide section used for this report.

$$W/m = \int (W/m^2)(s)ds. \qquad (2.4)$$

For the present report all integration is from s=0 to s=31 cm. This is the region defined as the "gasket region". The procedure therefore allows great flexibility in defining the gasket region dimensions. Once the heat leakage is obtained in W/m this value can simply be divided by the *experimentally* measured temperature difference.

The methodology developed allows for the determination of the gasket region heat leakage per unit length and per unit temperature difference between the interior and exterior. The final results for five experiments with three different gaskets are summarized in Table 2.4. Gasket 1 appears to be the most effective of the three gaskets tested. It produces the smallest heat leakage and the largest temperature difference.

Table 2.4: Time averaged temperature differences and heat leakages for the gasket region from the Blue Box experiments

Exp.	Heat Load (W)	Gasket	ΔT (K)	Heat Leakage (W/m.K)
1	9.2	1, Original	20.2	0.19
2	13.14		26.6	0.20
3	18.13		34.6	0.21
4	13.14	2, Black Side-by-Side	25.2	0.23
5	13.14	3, White	25.6	0.22

The approach described above rests on the assumption that there is a linear variation of the heat flux per unit length of the gasket region with the temperature difference. The desired heat leakage factor in units of W/m.K is after all the slope of the W/m along the surface as a function of the temperature difference. Its use therefore implicitly assumes linearity. This assumption was confirmed to hold for both the experimental data and for the CFD results; at least within the degree of uncertainty of the approach (note that Experiments 1-3 in Table 2.1 appear to have a slight increase of heat leakage with temperature difference but the differences are only 0.01 W/m.K). One means of doing this is to take all of the "raw" data and then non-dimensionalize it. Figure 2.18 presents all of the raw data plus the same data normalized by the gasket surface length (0.31 m) and the specific heat load for each case. The "collapse" of the data in Figure 2.19 of the figure confirms the linear scaling (as did other tests).

2.7. Future Improvement

Our first conceptual design was to build the Blue Box to better isolate a length of the gasket region than can be done in an actual refrigerator. We provided a literature review in which others have measured the gasket heat leakage in actual refrigerators using the reverse heat load method (placing a heating element inside the unit). They then place heat flux sensors on all inner surfaces, multiply each by its area, add up all the values and subtract from the input load. The original concept was that the heat flux distribution in a unit is far too complex to do this accurately. We first proposed to use the Blue Box to do the same. With a much simpler geometry the results should be more accurate. Unfortunately, it turned out to not be that simple. We placed heat flux sensors along all of the inner walls at 16 locations. By playing with the surface area attached to each heat flux measurement we could get any answer. So, to get accurate results we had to move the heat flux sensors to the outer surface and couple the methodology with CFD as described above.

For the future improvement we suggested that the box benefits from having a longer section of the exposed gasket. It should have the ability to be turned such that the gasket region is aligned vertically since convection in the vertical direction might have a significant effect on heat transfer. The Blue Box may also benefit from having a much longer portion of both door and wall pieces exposed to the ambient rather than just the 31 cm section used for the prototype. Whereas the first concept benefited from having as much insulation as possible this is not as important under the current methodology. Having larger sections of the door and wall exposed could create a more natural flow of heat through the gasket region as well as allow the measurement of both the gasket and the wall/door away from it. Any design changes though should retain a symmetric flow/heat transfer profile

such that only 2D CFD is needed for the shape factors. In addition, the current Blue Box has an interior made entirely of wood. Therefore, great care must be taken to not heat the box to dangerous temperatures. This is particularly true since the box is left unattended for days at a time. Searching the literature suggests that the internal temperature can be quite high, but some evidence exists for smoldering as low as 80 ^{0}C (albeit for much longer times). Another safety precaution would be to simply line the interior of the box with a fire retardant material.

2.8. Summary

A comprehensive methodology for experimentally determining heat leakages through gasket regions of refrigerators has been developed. The process involves using the "Blue Box" to isolate the heat transfer through only the portion of the gasket region that is of interest. Heat flux sensors are then placed along the outer perimeter of the gasket region and thermocouples are used to measure temperatures inside and outside of the box. The box has a heating element inside which heats the box to steady state using the "reverse heat load" method. The six heat flux sensors do not have the resolution necessary to fully resolve the surface heat flux distribution. Therefore, two dimensional (2D) computational fluid dynamics (CFD) is used to provide "shape factors" of the surface heat flux that are then best fit to the experimental data. Once integrated and divided by the temperature difference these profiles provide the heat leakage per unit gasket length, per unit temperature difference. The methodology has been used to test three gaskets and shown to be sufficiently accurate to determine differences in different gasket behaviors (Table 2.4). Note that the door sections are removable and any set of doors can be cut and placed within

the Blue Box for measurements. Finally, additional CFD were conducted which show that the addition of a freezer fan increases the experimentally determined heat leakage values by approximately 20%. The further addition of a hot pipe increases these values by a further 10%.

3. EXPERIMENTAL INVESTIGATION ON AIR LEAKAGE FOR DOMESTIC REFRIGERATORS

This research was conducted with the objective of developing an experimental methodology to identify and measure air exchange flow rates and corresponding heat leakages in commercial refrigerators due to air leakages. The idea for this project started with a journal paper written by Alfonso, Castro [17]. The paper measured air leakage rates and energy losses through both new and old gaskets on the same refrigerator. Only their results for new gaskets are pertinent to the present study. They found that the air changed over 1.1 times per hour through the freezer compartment and 2.1 times per hour through the fresh food compartment. They measured the effective heat transfer at 0.93 W and 2.35 W, respectively. The total loss reported, 3.28 W, is approximately 7% of the compressor power consumption averaged over an hour of operation, or approximately 3% of the compressor power consumption during operation.

The volumetric flow rates corresponding to these air change rates (I) are:

- for a freezer (subscript fr) having a volume (V) of 0.11 m^3, and

$$I_{fr} \times V_{fr} = 2\ {}^{Liters}/_{min} \tag{3.1}$$

- for a fresh food (subscript ff) having a volume of 0.41 m^3

$$I_{ff} \times V_{ff} = 14\ {}^{Liters}/_{min} \tag{3.2}$$

These values were used to specify the flow meter used in the current study. However, as shown below they are far larger than measured flow rates. Possible reasons for the errors in the paper are discussed below.

It was determined that the air intake was primarily through the water drain tube due to the presence of the fan during operation (Bernoulli's Equation: velocity goes up, pressure goes down, creating a low pressure region near the water drain tube inside the unit). However, we now understand that this is only part of the reason for the air intake. Air flows are predominantly cyclic with air mass inside of the cabinet increasing during compressor operation as the internal temperature decreases. This causes the air to become denser and therefore the cabinet gains air mass. After compressor operation the heavy air then "falls" back out of the cabinet. This is essentially a "breathing" and "exhaling" process.

Based on the above, three tasks for this project were to: 1) find the leaks and their relative importance, 2) measure the air leakages both in and out, and 3) calculate the energy losses associated with air leakage. This was to be done with one refrigerator in order to develop the proper methodology.

The First Law of thermodynamics for a control volume enclosing a refrigerator is:

$$\frac{\delta E_{cv}}{\delta t} = \dot{Q} - \dot{W} + [\sum \dot{m}_{in} h_{in} - \sum \dot{m}_{out} h_{out}] \tag{3.3}$$

where the term on the left represents the time rate of change of the total energy within the control volume, $\dot{Q}$ is energy transfer through heat transfer, $\dot{W}$ is the power consumption by the compressor, and the final term in brackets represents the net energy increase or decrease

due to air infiltration ($\dot{m}$ being the mass flow rates, and h being the enthalpy). Note that changes in potential and kinetic energy have been neglected in the bracketed term. This assumption has been verified to be valid and is widely used in studies such as the present one. The focus of this study is the last term in brackets; i.e. determining the effective energy gains or losses due to air flow through leakages:

$$\dot{Q}_{eff} = \sum \dot{m}_{in} h_{in} - \sum \dot{m}_{out} h_{out} \tag{3.4}$$

The primary problem in directly measuring $\dot{Q}_{eff}$ in a refrigerator is in locating all of the possible leakage points, and then measuring the mass flow rates and temperatures (needed to obtain the enthalpies) of all of them. However, we have developed two methodologies to measure $\dot{Q}_{eff}$. The first involves completely sealing a refrigerator leaving only a single inlet and a single outlet for which we can measure the mass flow rates and temperatures. The two holes are sized to mimic operating conditions measured in an unsealed unit. The second is based on mass conservation and only requires knowledge of the internal air temperatures as a function of time and the internal freezer and fresh food volumes. Given a proper flow meter the first approach will be more accurate since the latter approach involves neglecting additional volumes within the cabinet that air can occupy and having to estimate the average temperature at which air exits the cabinet.

3.1. Methodology 1

The presented methodology requires two experiments to measure the air and energy losses directly. The first law of thermodynamics shows that the energy loss due to leakages is the sum of all the mass flow rates out multiplied by the enthalpy of the air at each temperature minus the same for the inflows. This approach neglects changes in potential and kinetic energy; however, these have been calculated and shown to be negligible. This methodology is considered to be accurate given the proper equipment. However, a second methodology described below shows that the flow meter currently used is not sufficiently accurate for the actual flow rates that are predicted indirectly through the second approach based on mass conservation.

3.1.1. Experiment 1

For the first experiment, we have one unsealed (normal operating) unit that has a single obvious leakage path to the freezer through the drain tube. However, as shown below, there are many additional leakages of unknown size and relative importance. The first law cannot be directly used to calculate all of the mass flow rates and associated temperatures needed to find the enthalpies. Therefore, this experiment is used solely to measure normal operating conditions needed to mimic the real refrigerator conditions in the second unit discussed next (pressure differences between the freezer and fresh food compartments and the ambient, temperatures, and the normal compressor operating cycle time).

3.1.2. Experiment 2

Therefore, we have a second identical, but completely sealed, unit - other than the drain tube and a second hole drilled in the wall of the fresh food compartment. The procedure for sealing the unit is discussed later. We adjusted the hole size until we were getting the same pressure differences between the freezer and fresh food compartments and ambient measured in the real unsealed conditions. This essentially recreates the operating conditions of the unsealed unit by providing an equivalent leakage area. We now can directly measure the single inflow mass flow rate with a flow meter and the single mass flow rate out along with both temperatures needed to find the enthalpies. Mass flow rates are obtained by multiplying the measured volumetric flow rates by the density of the air calculated from the ideal gas law. With the single inlet – single outlet, calculating the energy loss due to air infiltration is straightforward:

$$\dot{Q}_{eff} = \sum \dot{m}_{in} h_{in}(T_{in}) - \sum \dot{m}_{out} h_{out}\,(T_{out}) \tag{3.5}$$

where $\dot{Q}_{eff}$ is the effective heat transfer rate, T_{in} is the room temperature at the drain tube inlet, and T_{out} is the fresh food temperature at the exit hole (both being measured with thermocouples).

Figure 3.1: Pictures of the sealed unit.

3.1.3. Experimental Data Collected

Experimental data recorded for this project includes temperatures, pressure differences, and inflow and outflow flow rates for both an original and sealed units. Figure 3.1 shows pictures of the experimental apparatus for the sealed unit. Figure 3.2, Figure 3.3 and Figure 3.4 show internal temperatures and pressure differences measured from the unsealed freezer and fresh food compartments as functions of time. Very accurate low pressure transducers were used to measure the actual pressure difference between both the freezer and fresh food compartments and the ambient. The differential transmitter used

for getting the pressure measurements had ±0.25% accuracy and the operation rage was ±0.05 inches of water.

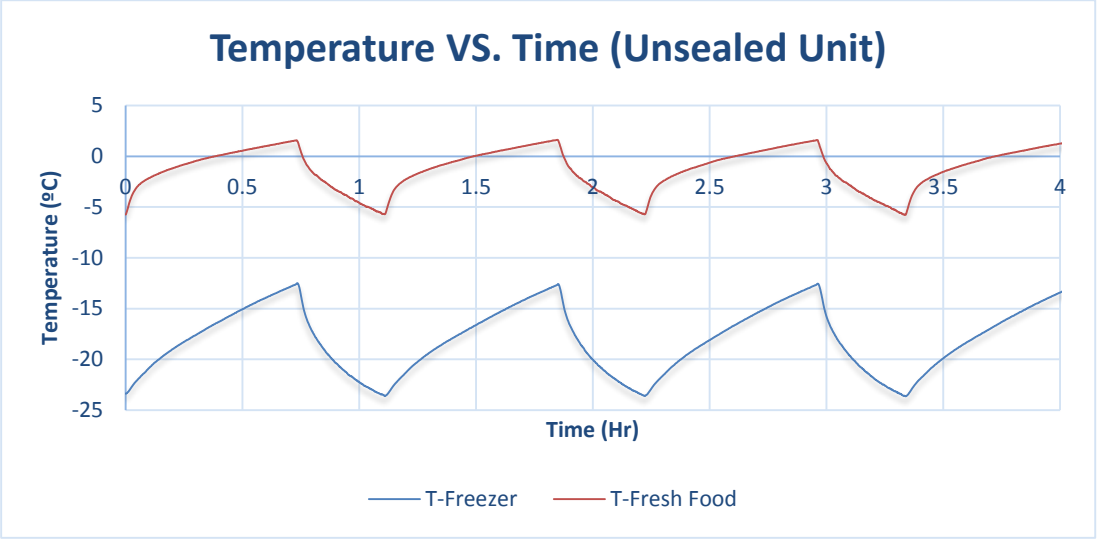

Figure 3.2: Example data for the temperature of **unsealed** fresh food compartment and freezer compartment

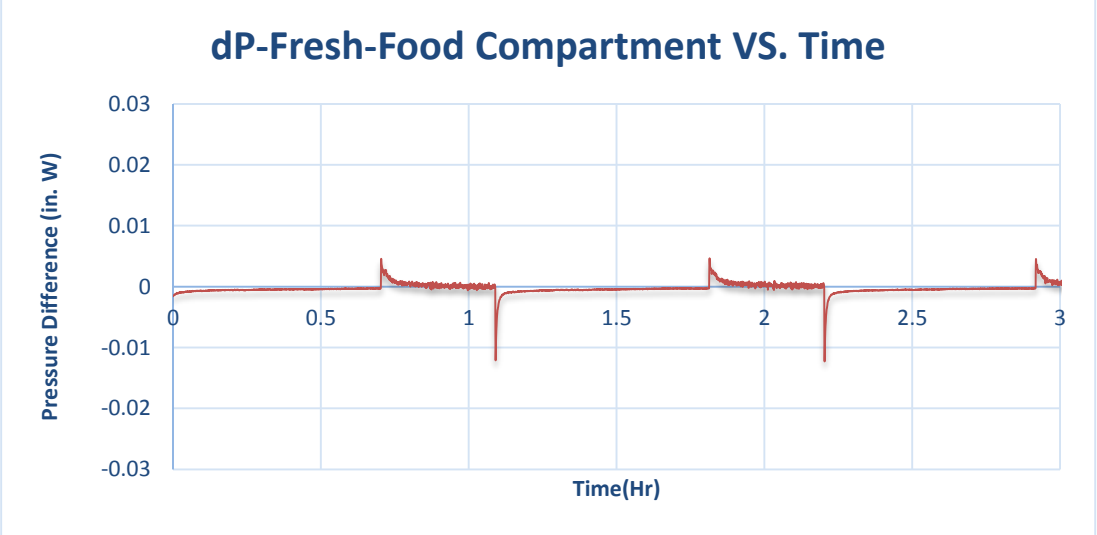

Figure 3.3: Example data for pressure difference between the **unsealed** fresh food compartment and ambient as a function of time.

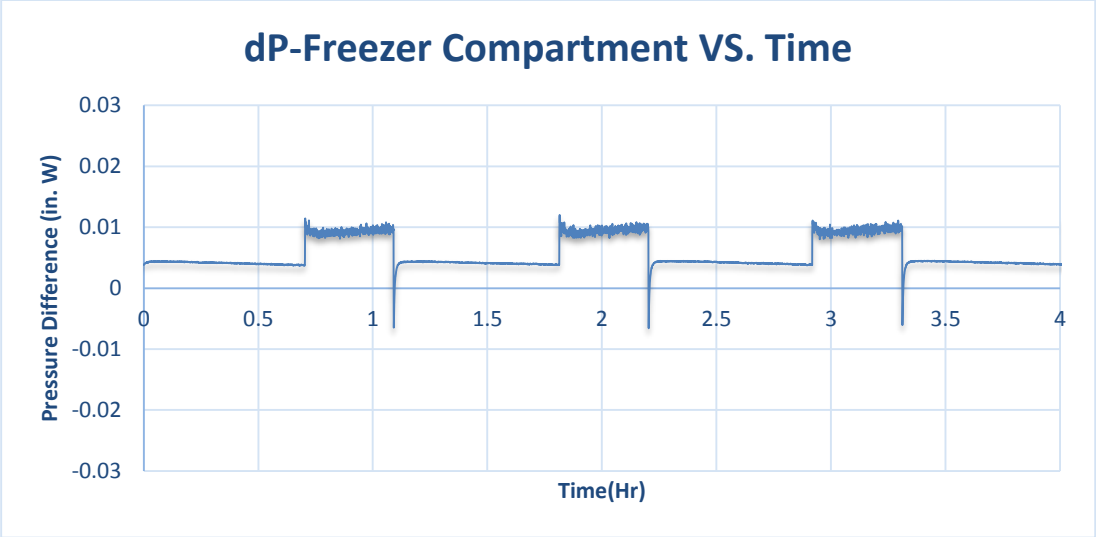

Figure 3.4: Example data for pressure difference between the **unsealed** freezer compartment and ambient as a function of time.

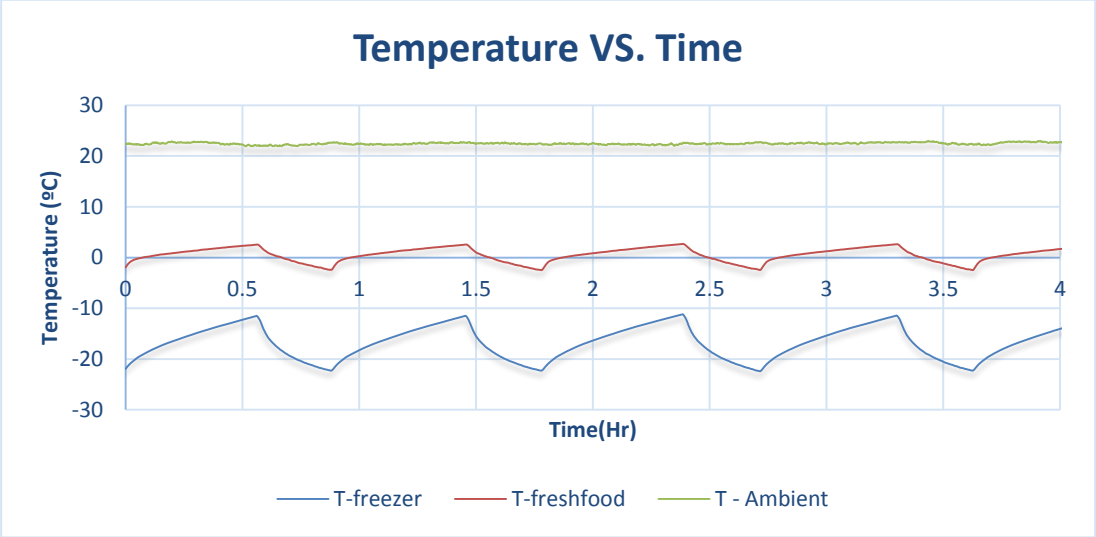

Figure 3.5: Example data for the **sealed** refrigerator air temperature entering the unit from the room and exiting the unit through the fresh food compartment as a function of time. These are the temperatures used to calculate the inflow and outflow enthalpies

Although the presented data were gathered during multiple realizations, each figure is scaled to begin with the end of the compressor operation for ease of comparison. Figure 3.5 presents the temperatures within the cabinet sections as well as the ambient temperature measured at the intake at the drain tube. This ambient is used to calculate the intake air enthalpy as described below. The outflow enthalpy is obtained from the fresh food compartment temperature. Figure 3.6 and Figure 3.7 present the horizontal pressure differences between the fresh food and freezer compartments relative to outside ambient, respectively.

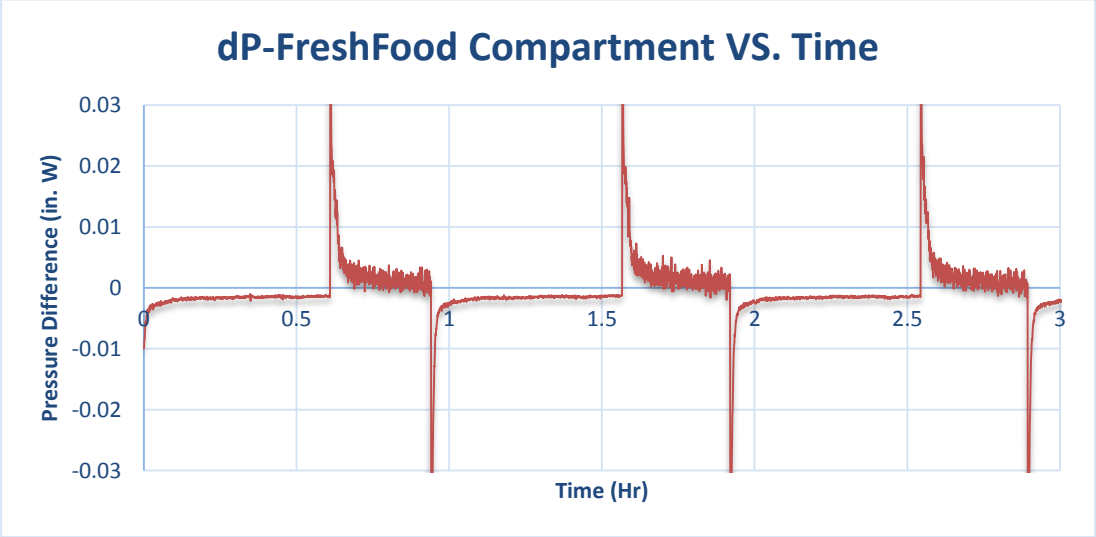

Figure 3.6: Example data for the **sealed** refrigerator pressure difference between the fresh food compartment and ambient as a function of time

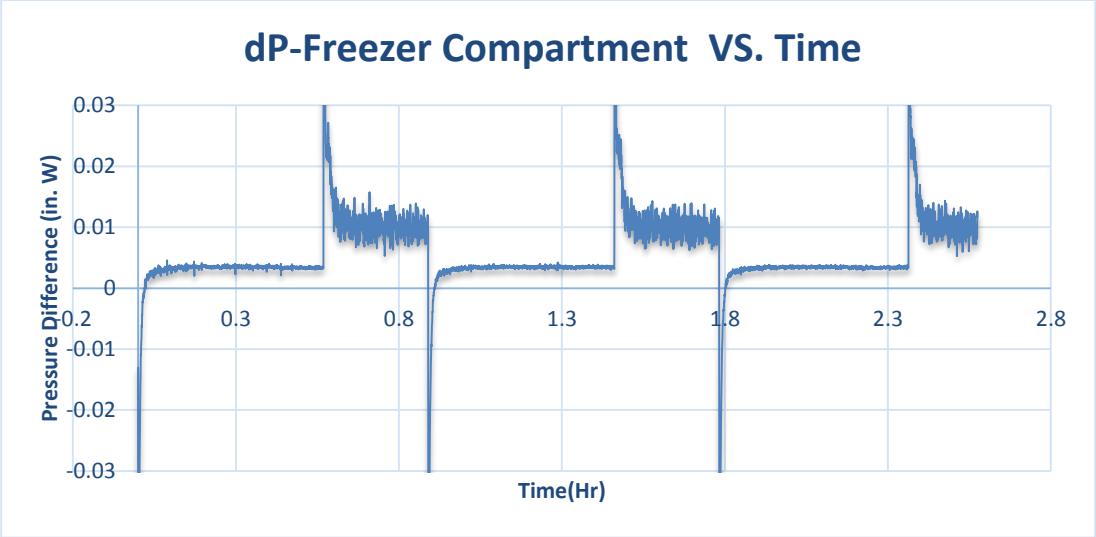

Figure 3.7: Example data for the **sealed** refrigerator pressure difference between the fresh food compartment and ambient as a function of time

Positive values indicate that the pressure inside the cabinet is lower than ambient. A comparison with the pressure differences for the unsealed unit (Figure 3.3, Figure 3.4) shows good agreement during operation. The only significant difference is at the moments when the compressor either starts or shuts down. These "spikes" are considered negligible to the conclusions of the study.

Finally, flow rates as a function of time are presented for the sealed unit in Figure 3.8, Figure 3.9 and Figure 3.10. Both Figure 3.8 and Figure 3.9 are for the inflow at the water drain entrance. The DAQ was unable to record negative flow rates so the zero values in Figure 3.9 represent unknown possible outflows. Therefore, the flow meter was reversed to gather the outflow data as shown in Figure 3.9. The spikes in Figure 3.9 represent the end of compressor operation. At that point the cold dense air within the unit simply "falls" outside through both the drain tube and the exit hole in the fresh food

compartment as shown in Figure 3.9. Other than that, the outflow through the drain tube is negligible.

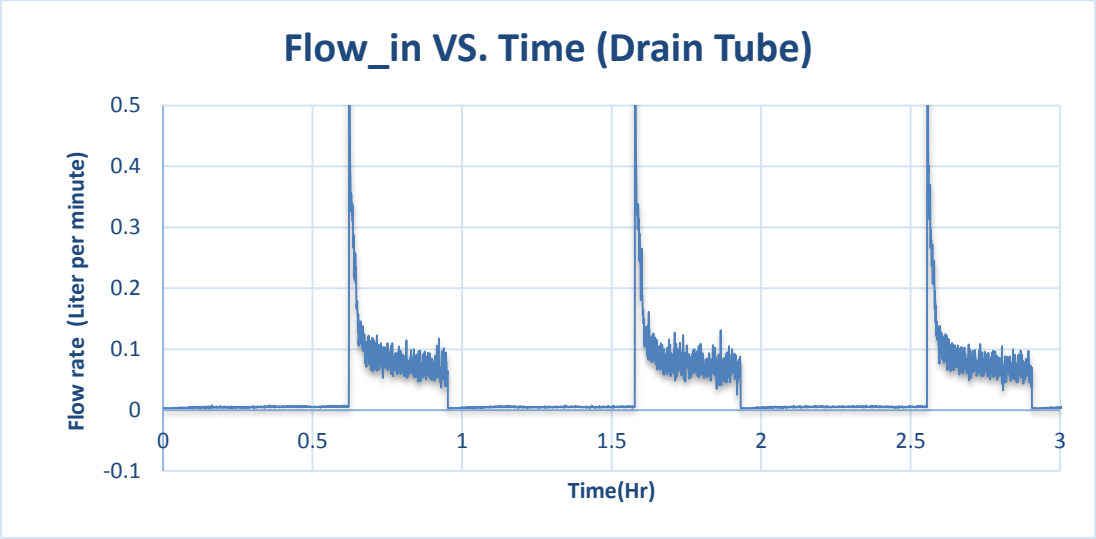

Figure 3.8: Example data for the sealed refrigerator air flow rate entering the drain tube as a function of time

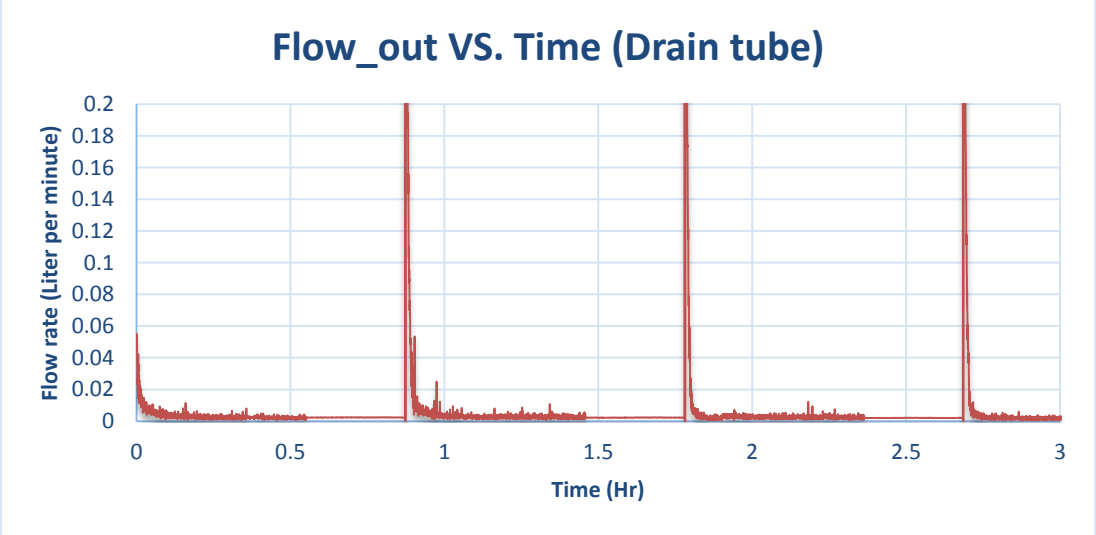

Figure 3.9: Example data for the sealed refrigerator air flow rate exiting the drain tube as a function of time.

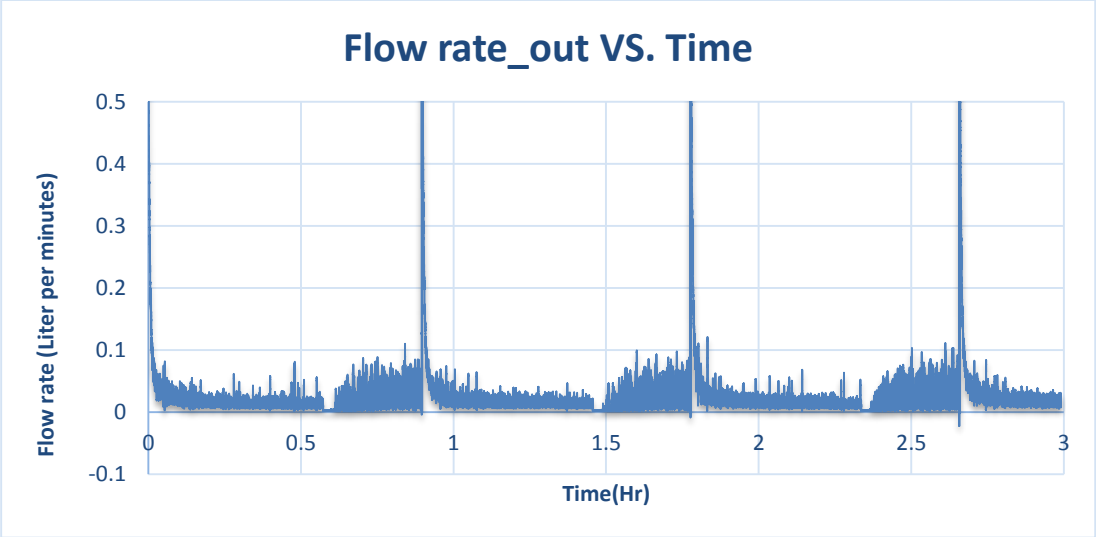

Figure 3.10: Example data for the sealed refrigerator flow rate exiting the fresh food compartment via the drilled hole as a function of time.

Two primary issues with the data presented in these figures are to be noted. First, there is good agreement with the operating pressure differences between the unsealed and sealed units. The outflow hole for the sealed unit was sized to match the pressure differences. The only exception is at the start and stop of the compressor cycle when the sealed unit experiences momentary large spikes not observed for the unsealed unit. The second issue is observed in Figure 3.8 and Figure 3.10. The flow meter purchased has a range of 0 to 15 liters / min. This was based on the Alfonso and Castro 2010 paper [17] but proved to be far too large a range for the measured operating conditions (the reason the paper is considered to be incorrect is discussed below). As these figures show there is considerable uncertainty in the measured flow rates which are well within the noise level of the flow meter. For current purposes we are estimating the operating intake flow rate to be 0.075 liters / min (Figure 3.8) and the out flow to be 0.025 liters / min (Figure 3.10). This can be easily improved upon by purchasing a flow meter with a range of 0 to 1 liter /

min. As the purpose of the present work is primarily on developing the methodology the current uncertainty is not considered overly important to the conclusions of the study.

3.1.4. Example Calculations

In order to calculate the energy leakage rates due to air infiltration only data for the inlet and outlet flow rates and temperatures (enthalpies) are needed from the sealed refrigerator:

$$\dot{Q}_{eff} = \sum \dot{m}_{in} h_{in}(T_{in}) - \sum \dot{m}_{out} h_{out}\,(T_{out}) \tag{3.6}$$

These data are found in Figure 3.5, Figure 3.8 and Figure 3.10. In theory $\dot{Q}_{eff}$ can be calculated as a running function of time if all of the data are collected simultaneously and if the enthalpy of the air as a function of time is available within the software. This should be done in practice in order to determine the net energy losses over an entire operation cycle. We did not have sufficient equipment to collect all data simultaneously so only a single example calculation is provided during compressor operation (at which point energy loss rates are maximal). We use the intake flow rate to be 0.075 liters / min (Figure 3.8) and the out flow to be 0.025 liters / min (Figure 3.9) during compressor operation as mentioned above. Mass flow rates are obtained by multiplying by the density. The density is calculated from the temperature using the ideal gas law: $\rho = \frac{P}{RT}$, where ρ is density in kg/m^3, P is standard atmospheric pressure 101325 Pa (pressure differences are approximately 1-2 Pa and completely negligible), R = 287 J/(kg.K) is the specific gas constant, and the temperature T is in K. We use T_{in} = 295.5 K and T_{out}= 274 K from

Figure 3.5 near the end of compressor operation (note again the time dependence). At these temperatures the corresponding enthalpies are h_{in}= 295 kJ/kg and h_{out}= 275 kJ/kg. The calculated mass flow rates and heat leakage after proper unit conversion are:

$$\dot{m}_{in} \approx 1.5 \times 10^{-6} \text{ kg/s}$$

$$\dot{m}_{out} \approx 5.4 \times 10^{-7} \text{ kg/s}$$

$$\dot{Q}_{eff} \approx 0.3 \text{ W}$$

This, again, represents an approximate value for the maximum energy loss rate during compressor operation. As mentioned above, an average over an entire cycle would provide more useful information.

One indirectly related issue is a compressor power consumption comparison of the sealed refrigerator when running with the two holes opened vs. when the two holes are sealed. This data is provided in section 3.10.

3.2. Methodology 2

The above calculation shows that the outflow mass flow rate is substantially less than the intake mass flow rate. At first thought it may seem that the unit is not completely sealed and that additional mass flow rates in or out have not been accounted for. However, the explanation is that the process is not steady. As the air is being cooled during compressor operation (Figure 3.5) the density of the air is increasing and the unit is accumulating air mass. In contrast, after compressor operation the temperatures rise within the cabinet forcing air out as it expands. This is very similar to a "breathing" cycle. Therefore, a proper unsteady mass balance must be considered. At any given time:

$$\frac{\delta M_{cv}}{\delta t} = \dot{m}_{in} - \dot{m}_{out} \tag{3.7}$$

where $\frac{\delta M_{cv}}{\delta t}$ is the time rate of change of the total mass of air within the control volume defined by the outside surface of the refrigerator. This term can be decomposed as:

$$\frac{\delta M_{cv}}{\delta t} = \frac{\partial m_{fr}}{\partial t} + \frac{\partial m_{ff}}{\partial t} + \frac{\partial m_{add}}{\partial t} \tag{3.8}$$

or:

$$\frac{\delta M_{cv}}{\delta t} = V_{fr} \frac{\partial \rho_{fr}}{\partial t} + V_{ff} \frac{\partial \rho_{ff}}{\partial t} + V_{add} \frac{\partial \rho_{add}}{\partial t} \tag{3.9}$$

where V_{fr} is the freezer compartment volume (0.11 m^3) V_{ff} is the fresh food compartment volume (0.41 m^3), and V_{add} is the total additional volume that air can occupy within the control volume (the aforementioned volumes be strictly the manufacturer's defined useable volume).

The mass rate gains during compressor operation (or losses between operations) can be calculated by approximating the derivatives as incremental changes in densities divided by their corresponding time change increments, again using the ideal gas law to obtain densities. This can be done for the freezer volume and the fresh food volumes as both the volumes and temperatures are known. It cannot be calculated for the missing additional volume since neither the volume or the (average) temperature is known. For practical purposes this missing volume is neglected hereinafter. The fresh food and freezer temperatures are presented in Figure 3.11 and Figure 3.12, respectively, for one compressor cycle. These data correspond to the unsealed original unit (Figure 3.2). From this data the

instantaneous densities can be calculated from the ideal gas law assuming constant absolute pressure (measured pressure changes are 10^{-5} than that of atmospheric). This allows calculation of the instantaneous mass flow rates and the instantaneous $\dot{Q}_{eff}$ due to air infiltration. The effective energy transfer rates are then calculated as:

$$\dot{Q}_{eff} = \sum \dot{m}_{in} h_{(T_{in})} \tag{3.10}$$

during compressor operation while room temperature air is being entrained, and as:

$$\dot{Q}_{eff} = \sum \dot{m}_{out} h_{(T_{out})} \tag{3.11}$$

between compressor operation when the air is exiting the unit. Both $\dot{m}$ values are positive numbers in the above. Figure 3.13 presents the measured mass flow rate as a function of time calculated from the temperature. While the compressor is not operating the negative mass flow rate indicates flow out of the unit. Once the compressor turns on then the flow is reversed and enters the unit. For the enthalpy flowing out of the unit a mass weighted average temperature is used between the freezer and fresh food temperatures:

$$T_{out} = \frac{\rho_{fr} T_{fr}}{\rho_{out}} + \frac{\rho_{ff} T_{ff}}{\rho_{out}} \tag{3.12}$$

The energy transfer rates due to the air infiltration is presented in Figure 3.14 for the same one cycle period used in Figure 3.11, Figure 3.12 and Figure 3.13. Both mass and energy are exiting the unit while the compressor is off due to leakages. This does not indicate cooling. It is simply the energy associated with the exiting air mass. Energy is entering during compressor operation due to the intake of warm room temperature air with relatively large peak rate values as the compressor starts (≈13 W; see Figure 3.14).

However, when averaged over the time the compressor is operating the new result is $\dot{Q}_{eff}$ ≈ 4.4 W.

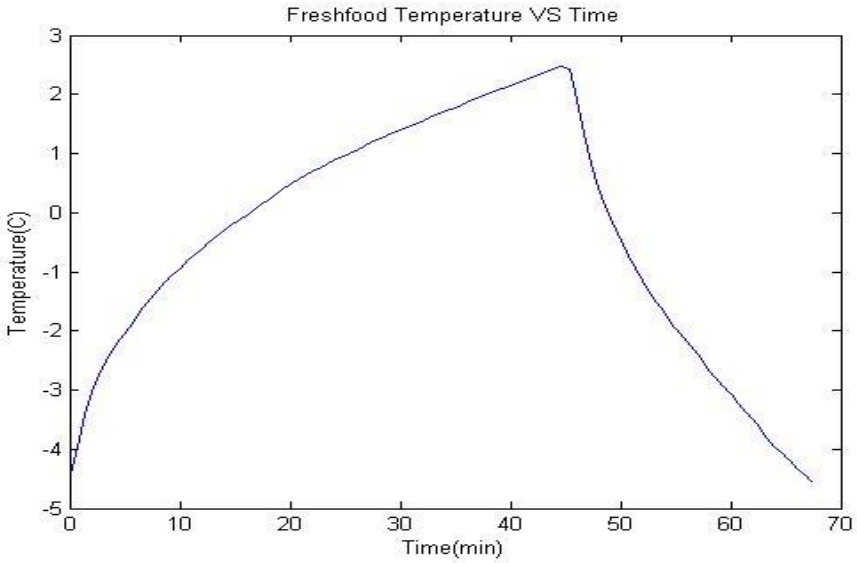

Figure 3.11: The fresh food compartment temperature as a function of time for the original unsealed refrigerator over one compressor cycle.

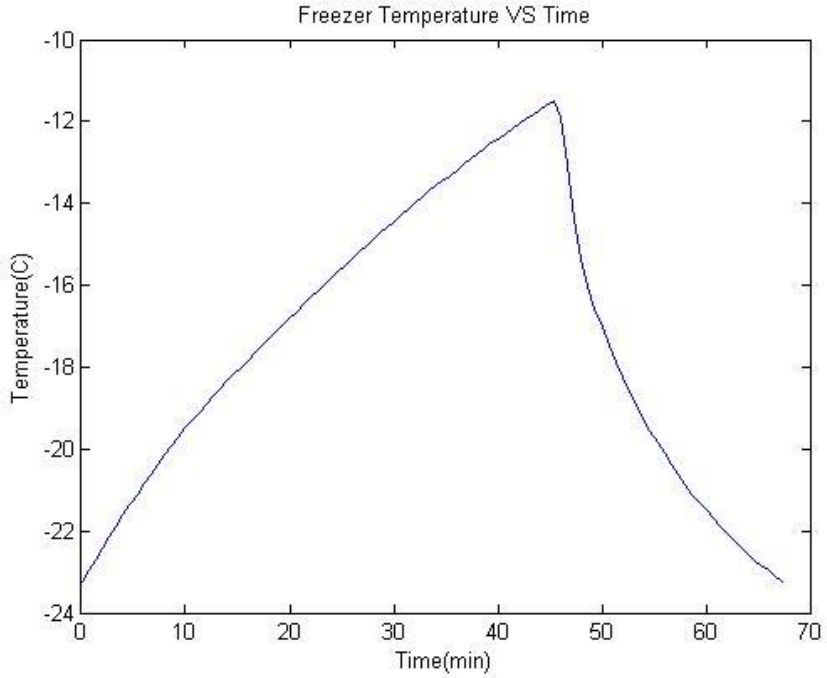

Figure 3.12: The freezer compartment temperature as a function of time for the original unsealed refrigerator over one compressor cycle.

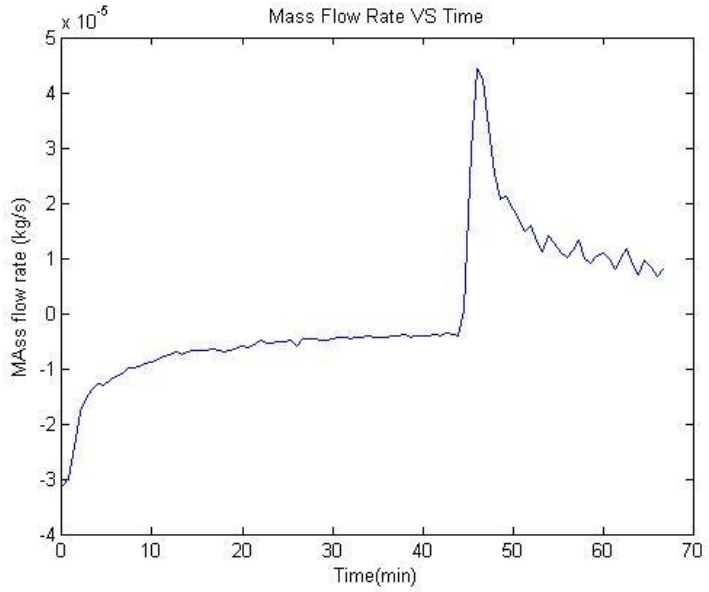

Figure 3.13: The mass flow rate into and out of the unit calculated from the temperature changes as a function of time for the original unsealed refrigerator over one compressor cycle (positive indicates into the unit).

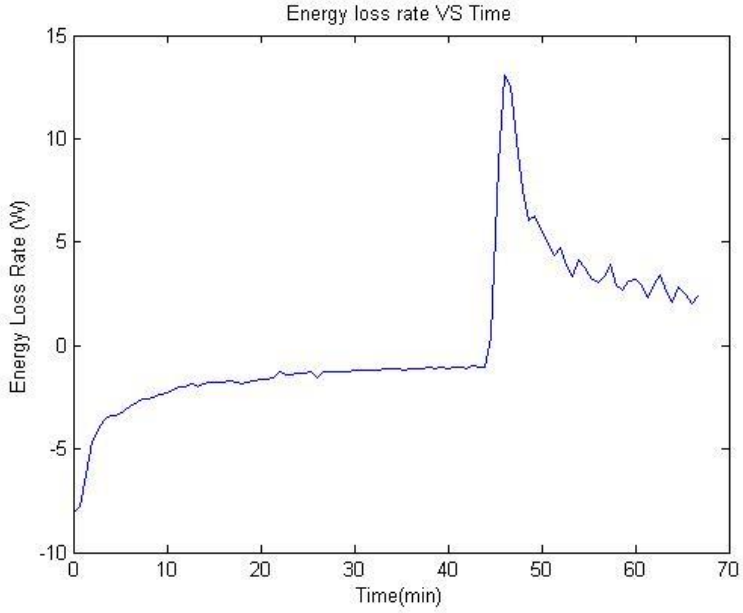

Figure 3.14: The energy transfer rate into and out of the unit calculated from the temperature changes as a function of time for the original unsealed refrigerator over one compressor cycle.

Positive indicates into the unit. Negative values occur between compressor cycles but do not represent cooling. They are simply due to cold air mass losses and their associated energies.

3.3. Alfonso and Castro 2010 and the Effects of Pressure Differences on Sealing the Unit

Even relatively small pressure differences acting over large surfaces result in very large forces. Consider a 1 psi (6895 Pa) pressure difference acting over a refrigerator door say 2 foot by 3 foot. That's 864 lbf (3843 N) of force. So, it was tried to pull a vacuum (or pressurize as we did) using a standard vacuum pump it produces pressure forces so large that the air simply forces its way through any available leakage path. The purchased standard pump produces either 10 psi of vacuum pull or 25 psi of pressurization. We were able to reduce the applied pressure down to 0.14 psi (960 Pa) and were able to find and seal enough of the holes for the unit to hold 0.11 psi. But, on that same hypothetical door this is still 120 lbf (540 N) *if the applied pressure held*. In order to understand the leakage rates through missing holes would require applying actual operating pressure difference, which we cannot do due to their very small values as discussed further below.

During compressor operation, the pressure difference induced by the fan in the freezer is only about 0.0003 psi (2.0 Pa) [0.25 lbf (1.1 N) on the 2' x 3' door]. Although we cannot produce that pressure artificially to confirm that we now have approximately zero flow rate for our sealed unit, we have essentially confirmed it under operation. This is further confirmed quantitatively below.

The "orifice equation" shows that the flow rate scales with the square root of the pressure difference. Therefore, as we reduce the pressure difference linearly the flow rate

reduces quadratically. We've now measured the actual flow rate entering the unit through the drain tube to be approximately 0.075 liter per minute (Figure 3.8) – although not correct due to the meter's accuracy. A better estimate from the mass conservation experiment is 0.6 liters per minute. This is a factor of 25 lower than would be needed to get the results from the Alfonso and Castro paper. That means that the refrigerator in the paper had a pressure difference about 5 times that of our unit (square root). Evidence that the paper has substantial error includes:

- They used a tracer gas decay rate to determine the air leakage rather than measuring it directly as we are doing. To start the experiment they have to pump the tracer gas in. This will increase the pressure inside. They did not measure any pressure differences. It's not too difficult to see how they could have raised the pressure difference from 0.0003 psi (2.0 Pa) to 0.0015 psi (10 Pa) (factor 5) (as an example). This alone would raise the air flow rate by a factor of 25 and be consistent with the results presented in the paper.
- We've found that the mass of air inside the unit "breathes" in cycles – in during compressor operation and out between. Alfonso and Castro [17] assumes that the system is in steady state with no accumulation. They calculate their energy losses using a single $\dot{m} = \dot{m}_{in} = \dot{m}_{out}$
- Furthermore, if we pump air in through the drain tube at the flow rate needed to produce the air turn over times reported in the paper it's very obvious that it is too large (you can feel the air blowing out along the gasket edges easily).

3.4. The Hypothetical Completely Sealed Refrigerator

Assuming one could completely seal a refrigerator from air leakages the behavior of the unit would change dramatically is the same set thermostat temperatures remained unchanged. For a completely sealed unit the density of the air inside would have to remain constant. In this case, temperature changes would result in pressure changes rather than density changes. Figure 3.2 provides the following minimum and maximum temperatures for the original unsealed unit:

$$T_{fr_{min}} = 250 \text{ K}$$

$$T_{fr_{max}} = = 260 \text{ K}$$

$$T_{ff_{min}} = 268 \text{ K}$$

$$T_{ff_{max}} = 275 \text{ K}$$

So, assuming that the unit starts at time 0 with one standard atmosphere of pressure and at the maximum temperatures the densities in the two compartments would be:

$$\rho_{fr\_0} = \frac{P_{atm}}{RT_{fr\_max}} = 1.36 \text{ kg/m}^3 \quad (3.13)$$

$$\rho_{ff\_0} = \frac{P_{atm}}{RT_{ff\_max}} = 1.28 \text{ kg/m}^3 \quad (3.14)$$

In which case the change in pressure during a compressor cycle to the minimum temperatures would cause pressure changes of:

$$\Delta P_{fr} = P_{atm} - \rho_{fr\_0} R T_{fr\_min} = -3{,}745 \text{ Pa} = -0.54 \text{ psi} \quad (3.15)$$

$$\Delta P_{ff} = P_{atm} - \rho_{ff\_0} R T_{ff\_min} = -2{,}872 \text{ Pa} = -0.42 \text{ psi} \quad (3.16)$$

If we assume that the freezer door has an area of 2 ft^2 and the fresh food compartment door has an area of 6 ft^2 this results in the following forces keeping the doors closed:

$$Force_{fr} = 690 \text{ N} = 155 \text{ lbf}$$

$$Force_{ff} = 2{,}870 \text{ N} = 360 \text{ lbf}$$

In reality the forces would be even larger as when the refrigerator is opened then closed the starting maximum temperatures would be even larger due to the door opening. The moral of the story is that while some energy can be observed by minimizing air leakages, too much minimization will eventually result in very large forces on the cabinet doors.

3.5. Future Improvements

For further measurements, we recommend having two flow meters and some additional equipment such that four temperatures (inflow, outflow, freezer compartment, and fresh food compartment) can be measured simultaneously. If all data is taken during a single simultaneous run of the experiment then the time dependent rate of energy loss through air infiltration can be directly measured as a function of time (rather than estimated

at single times when multiple runs have to be made). This would allow the average energy losses associated with air flows over an entire cycle to be calculated.

A higher quality lower pressure flow meter must also be purchased. As mentioned above, the purchased flow meter was originally specified by the data in Alfonso and Castro 2010. We estimated approximately 15 liters/min net flow into the unit to recreate their specified air turn over times. However, actual measured flow rates are ~0.1 liters/min and well within the noise level of the flow meter. This is very important to gathering accurate data as the flow rates being measured with the current flow meter are well within its noise range leaving substantial uncertainty in the measured energy leakage rates. Additional accuracy can be obtained by conducting the experiments in a psychrometric chamber as the inlet and outlet enthalpies and mass flow rates are affected by humidity.

3.6. Procedure for Sealing the Cabinet

Figure 3.15 shows our experiment configuration that we set up to pressurizing the refrigerator in order to detect any possible leaks. An air compressor, pressure tank, pressure regulator and pressure gauge are used to pressurize the system at the certain pressure. A flowmeter is also installed to measure the flow rate in this test configuration. A pressure pump creates a 25 psi air pressure at the outlet which is routed through pressure tank to control oscillations. Afterwards, air flows toward the safety valve and pressure regulator. The pressure regulator is reducing the air pressure to a suitable pressure so that the desired flow rate is obtained at the flowmeter. 0.14 PSI is found as a proper pressure which provides enough air flow and air pressure that let us detect the leaks visually by applying

bubble soap and looking for the bubble formation. High pressure air is entering the unit through the water drain tube.

Figure 3.15: The experimental set up for pressurizing the refrigerator to find and seal the leakages.

Obviously, air escaped from the gasket and any existed gaps until all leaks get sealed on the cabinet. The initial step was taking the doors off, filling up any obvious gaps with silicon and letting it dry out. Also, taking the hinges off and filling up the holes with silicon is necessary. The doors should be put back on the cabinet and be tighten by wrap ratchet straps. It is helpful to inject some silicone at the gasket edges while the ratchet straps are strongly tighten. Also, all the corners and edges on the back, bottom or sides of the unit should be taped by HVAC tape. We found HVAC tape as a very strong tape being able to make the gaps air tight against the applied air pressure.

Once the cabinet is completely sealed, the pressure regulator should be set on a certain pressure value (we found 0.14 psi suitable for our application). The high pressure air is entering the unit via the water drain tune so that the unit is pressurized. Now, pressure gauge should be monitored to make sure if the gauge shows the exact pressure set on the pressure regulator proving that the unit is air tight. Keep sealing the unit till the pressure gauge shows the pressure set on the pressure regulator.

Almost all gaps due to the electrical wiring are leaking; therefore, they should be filled up with foam and silicone. Likewise, all edges should be sealed with multiple layers of HVAC tapes.

(a)

(b)

Figure 3.16: (a) and (b) shows the major leakage paths

3.7. Getting Pressure Measurements from Refrigerator

Getting pressure measurements helps us understand the characteristic of the interior pressure behavior with respect to ambient pressure. Figure 3.17 shows the sample refrigerator that we selected to learn about its interior pressure behavior over a complete cycle. In this study, two high quality pressure transducers are measuring the pressure differences. The operation range of these pressure transducers are ± 0.05 (in. water column). Each pressure transducer is wired to an amplifier to improve the output signals and make a small pressure difference variations detectable for the DAQ system. Data is recorded on a computer via the DAQ system for further processing.

Figure 3.17: Images of the selected units - Top bottom

The pressure transducer is measuring the interior pressure of the refrigerator through a tube entering the cabinet via a hole drilled in the side wall. The pressure difference between the freezer and ambient and the pressure difference between fresh food compartment and ambient are measured separately. The pressure transducers being only capable of getting horizontal pressure difference measurements; i.e. they cannot measure hydrostatic pressure differences. Therefore, if the hydrostatic pressure difference exists, it should be added to the pressure measured by the sensors.

$$P_O - P_F = P_{F,O} \tag{3.17}$$

$$P_O - P_R = P_{R,O} \tag{3.18}$$

$$P_{F,O} - P_{R,O} = P_R - P_F = P_{R,F} \tag{3.19}$$

$$\Delta P_{Total} = P_{R,F} + \Delta P_{Hydrostatic} \tag{3.20}$$

$$\Delta P_{Hydrostatic} = \rho . g . \Delta h \tag{3.21}$$

Density of the air is a function of temperature. Therefore, it is more accurate to calculate the hydrostatic pressure between freezer and fresh food compartments from outside of the cabinet so that the temperature profiles are defined clearly at the inlet and outlet points; moreover, there is no air velocity to obscure the measurement due to dynamic pressures.

The mechanism of Top Bottom refrigerator was simple enough to understand. The compressor, evaporator fan and condenser fan start running to cool down the interior temperature simultaneously. There is a thermostat placed inside the fresh food compartment. Once the temperature in fresh food compartment reaches a certain value set on the thermostat, the compressor and the fans stop working. Therefore, the interior pressure in the refrigerator changes as follows: the pressure of the cabinet is getting lower and lower as the compressor is working and the cabinet is being cooled; however, the interior pressure is increasing over the idle cycle while the interior temperature is getting warmer.

The following plots show how inner pressure changes over idle and running cycles. The blue graph in Figure 3.18 shows the pressure difference between freezer compartment and ambient. According to the diagram, the minimum pressure in freezer compartment is measured when the compressor start running. It also shows the pressure of the freezer is always lower than the ambient pressure while the doors are closed and the compressor is

running. There is a spikes at a cycle showing that the pressure of the freezer compartment gets higher than ambient pressure once the compressor stop running. As soon as the compressor stops working, the interior pressure suddenly gets higher than the ambient pressure and then decreases quickly to a negative pressure value and remains almost steady till the compressor starts running again. Similarly, the red graph shows the pressure difference between the fresh food compartment and ambient. It illustrates that the pressure in fresh food compartment is behaving opposite. The pressure in the fresh food compartment is mostly higher than ambient pressure over the idle and running cycles. The pressure inside the fresh food cabinet increases as the compressor is operating so that the maximum pressure in the fresh food cabinet is recorded at the end of the operating cycle. However, there is a spike at a cycle showing that the fresh food pressure gets lower than ambient pressure for a couple of minutes at the beginning of the running cycle.

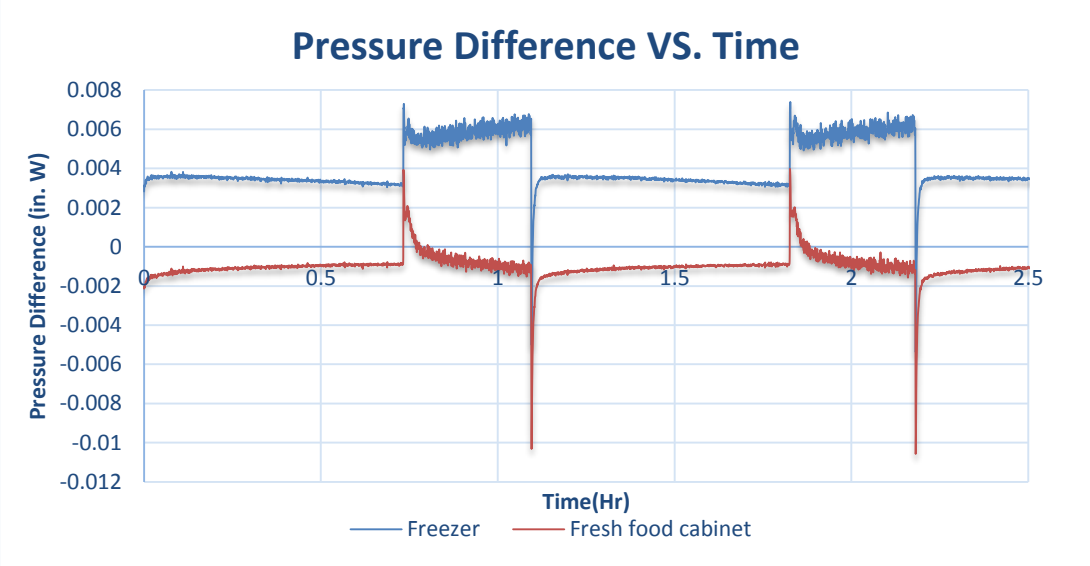

Figure 3.18: Difference of pressure between the cabinets and ambient.

Figure 3.19 illustrates how pressure difference changes between the compartments over two complete cycles. The graph proves that freezer pressure is always lower than the fresh food pressure. The lowest pressure difference between the freezer and fresh food compartments gets to 0.004 (in. W), but it is never disappeared. The pressure difference is increasing over the running cycle and the maximum pressure difference is as high as 0.007 (in. W). Accordingly, it can be claim that the pressure of the freezer is always lower than the fresh food compartment causing the air always naturally flows from fresh food compartment to freezer cabinet to compensate the pressure difference.

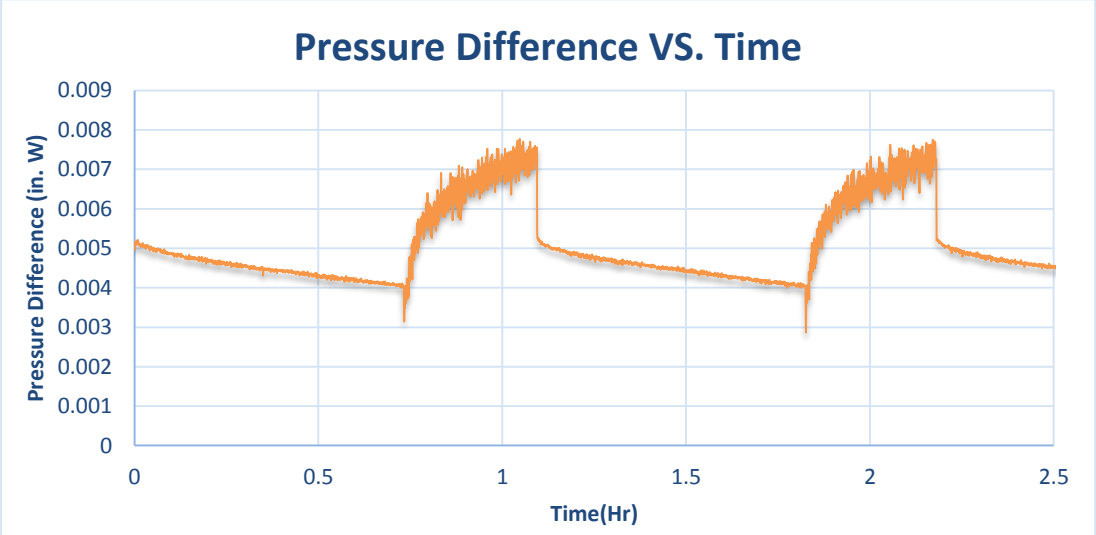

Figure 3.19: Pressure difference between fresh food cabinet and freezer without considering hydrostatic pressure.

3.8. Hydrostatic Pressure

As mentioned above, pressure transducers are not design to measure hydrostatic pressures between two points. Therefore, the procedure of the hydrostatic pressure calculation between the cabinets on top-bottom refrigerator is shown here. In the sample

refrigerator, hydrostatic pressure exists due to the height difference between freezer and fresh food compartments. Thus, hydrostatic pressure should be taken into consideration and added to the static pressure difference measured by the pressure transducers in order to get the actual pressure difference between these compartments.

$$\Delta P_{Hydrostatic} = \rho . g . \Delta h \tag{3.22}$$

The height difference between the drilled holes is 1.02 (m) and the density of the air is on the day of the experiment was 1.2 (kg/m^3).

$$\Delta P_{Hydrostatic} = 1.20 * 9.81 * 1.02 = 12.01 \text{ Pa} = 12.01 \ Pascal = 0.05'' \text{WC}$$

Following is the sample calculation showing how the actual pressure difference between the compartments varies over a cycle. Figure 3.20 shows the actual pressure difference between the compartments by considering their hydrostatic pressure difference.

$$P_{F,O,Max} \approx 0.007'' \text{ WC}$$

$$P_{R,O,Max} \approx -0.001'' \text{ WC}$$

$$P_{Max} = P_{F,O,Max} - P_{R,O,Max} + \Delta P_{Hydrostatic} \approx 0.058'' \text{ WC} \tag{3.23}$$

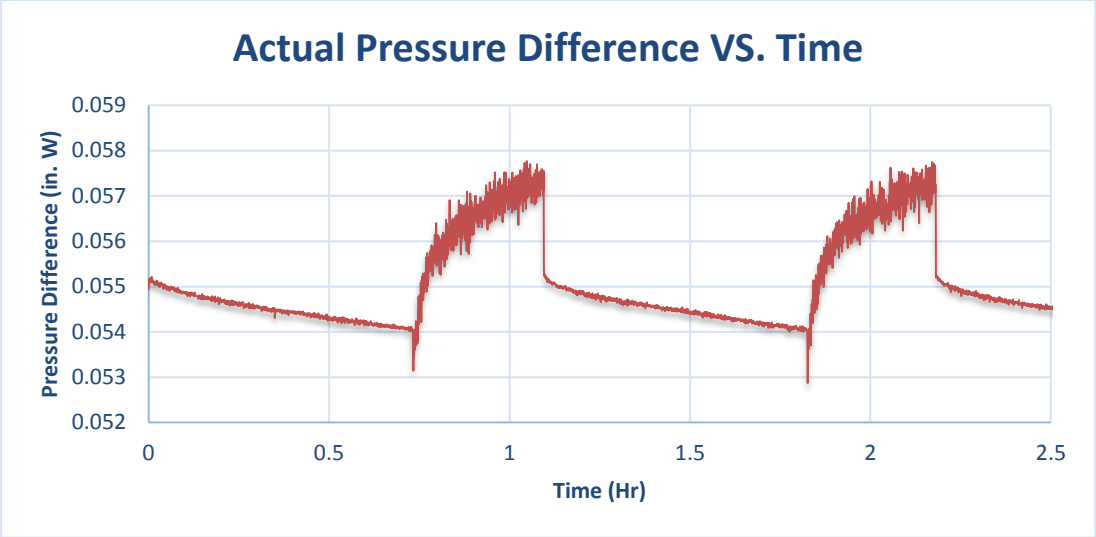

Figure 3.20: Actual Pressure difference between fresh food cabinet and freezer.

3.9. Closed Water Drain Tube

Water drain tube is known as one of the obvious and significant open air paths to the ambient environment. The pressure measurement was repeated with water drain tube closed to examine the influence of closing the drain tube on the pressure difference inside the cabinets. Figure 3.18 and Figure 3.21illustrate that sealing the water drain tube has no influence on the pressure difference of the cabinets. Figure 3.22 shows the actual pressure difference between the compartments with sealed water drain tube.

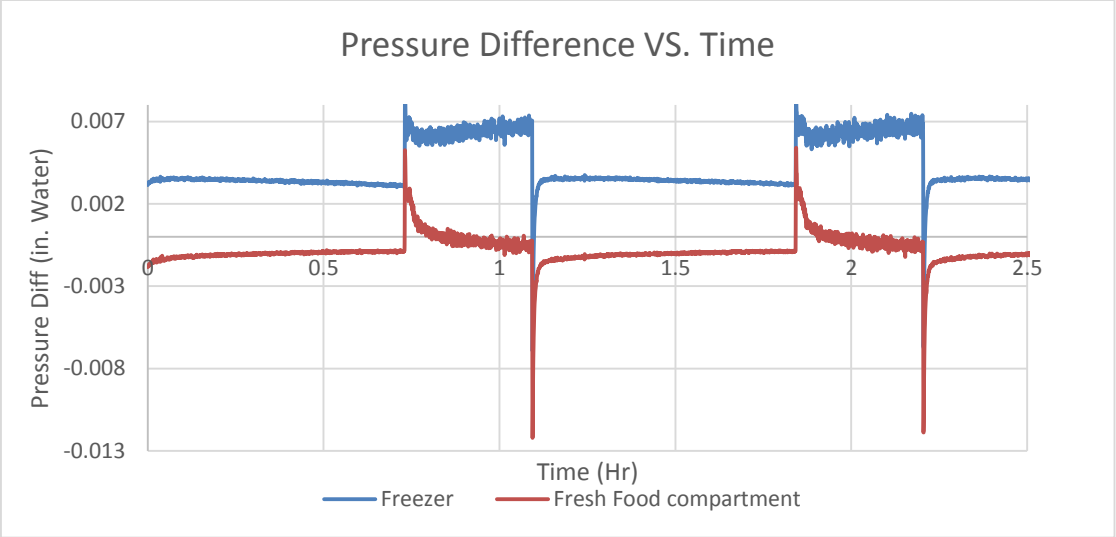

Figure 3.21: Difference of pressure between the cabinets and ambient with closed water drain tube.

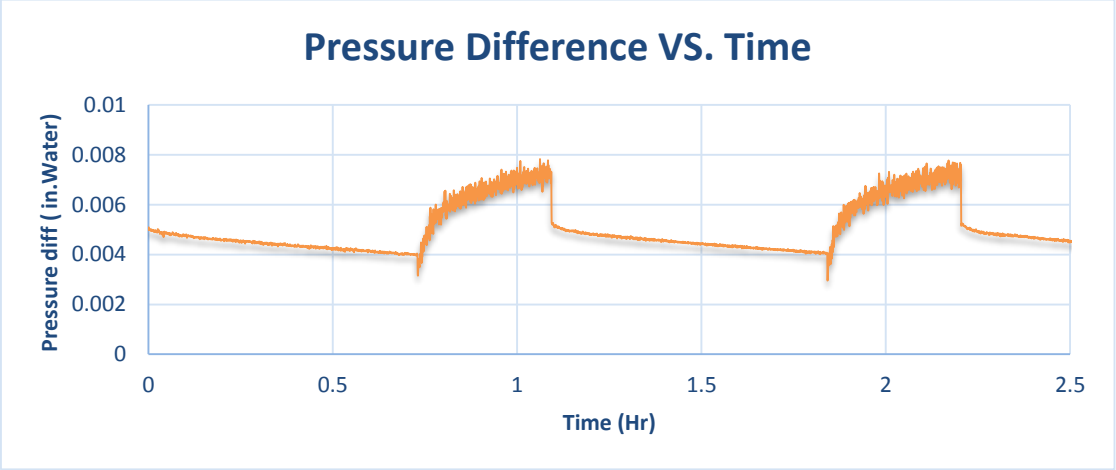

Figure 3.22: Pressure difference between fresh food cabinet and freezer without hydrostatic pressure.

3.10. Compressor Power Consumption for the Sealed Refrigerator

A voltmeter and a current sensor were measuring the power consumption of the refrigerator for a 24 hour. The measurements were made for the unit in two stages: 1) both the drain tube and the drilled fresh food compartment holes open, and 2) with both holes fully sealed. The results are shown in Figure 3.23 and Figure 3.24. It's difficult to draw conclusions as to whether the compressor runs for longer or shorter durations between open

and closed. The measurements were made at different times and perhaps with different room conditions (temperature, humidity). Some cycles are observed with both longer and shorter durations for the closed configuration. This makes some sense when considering the very large forces that would be created if the unit was truly 100% sealed. So, as the closed configuration begins operating it quickly creates pressures sufficient to find some small paths into and out of the unit. In addition, these were the last measurements made. The tape and other seals may have loosened over the weeks of measurements.

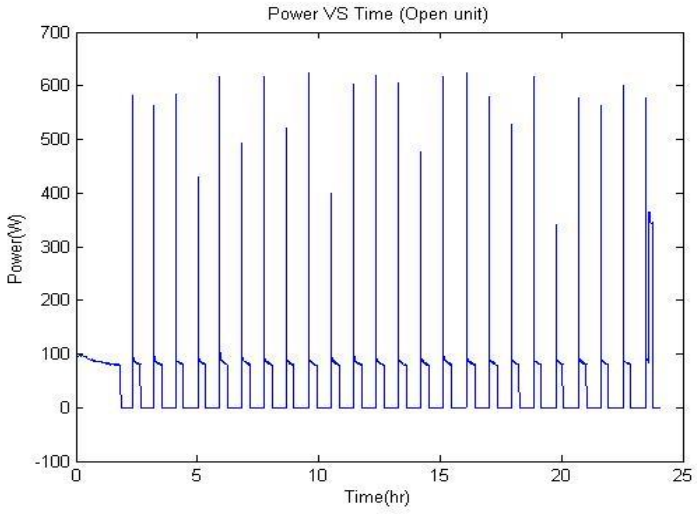

Figure 3.23: Compressor power consumption for the sealed refrigerator with the drain tube and drilled fresh food compartment holes open.

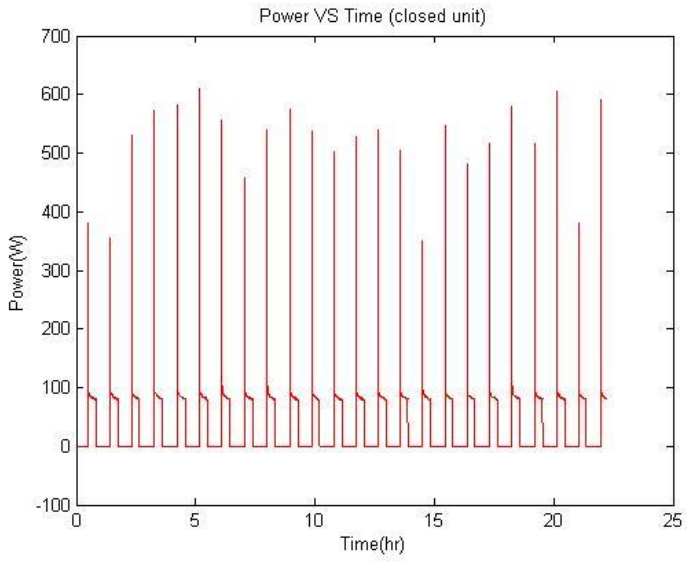

Figure 3.24: Compressor power consumption for the sealed refrigerator with the drain tube and drilled fresh food compartment holes closed.

3.11. Summary

The water drain tube was identified as a primary (but not the only) path for air to infiltrate the unit. This occurs due to the evaporator fan creating a low pressure point near the entrance to the tube within the freezer compartment as well as to the air temperature dropping thereby increasing the air density. The pressure difference between the freezer and fresh food compartments with respect to the outside ambient pressure was measured during normal operation on a given unit. The gasket and many other leakage paths were identified. Therefore, the entire unit was completely sealed using HVAC tape, expanding foam, silicone, and ratchet straps leaving only the water drain tube open. Next drill a hole through the wall of the fresh food compartment and adjust the diameter to match the originally measured pressure differences while operating. The hole acts as the single

effective leakage area of the original unit thereby replicating its behavior. This creates a single-inlet, single-outlet (SISO) system amenable to energy calculation. Then, flow rates and temperatures were measured at the inlet and outlet locations during operation. Given the two mass flow rates and temperatures the energy leakage due to air infiltration can be directly calculated from the first law of thermodynamics as $\dot{m}_{in}h_{in}(T_{in}) - \dot{m}_{out}h_{out}(T_{out})$, where the $\dot{m}$ is the measured mass flow rates at the inlet and outlet and the enthalpies, h, are obtained from thermodynamic tables at the measured temperatures.

As a conclusion, the methodology developed is sound and effective in measuring air infiltration and energy losses. The energy loss due to air leakages based on the flow meter approach estimates an upper energy loss rate of ≈ 0.3 W during compressor operation. An alternative approach based on calculating the air accumulation rate within the refrigerator directly from temperature measurements predicts a corresponding energy loss rate up to ≈ 13 W for a brief time at the start of compressor operation. When averaged over one compressor operation the effective heat transfer rate due to air infiltration is approximately 4.4 W. This latter value is a much better estimate as the data obtained with the flow meter are not mass conserving by nearly an order of magnitude. In addition, the air turn over times and energy leakage rates reported in "Air infiltration in domestic refrigerators: The influence of the magnetic seals conservation, Clito Alfonso and Manuel Castro [17], are incorrect and substantially over predicted. They predict air infiltration rates of ≈ 16 liters / min. We show this is not possible above. This value was used in specifying the flow meter purchased for the project. Actual values we measured are ≈ 0.1 liters / min on a flow meter scaled from 0 – 15 liters / min. Mass conservation dictates that the infiltration rate must be one order of magnitude larger. The only conclusion is that the

meter is completely inaccurate for these small flow rates. Moreover, during the compressor operation the pressure difference between the freezer and ambient was measured to be approximately 2.9 x 10^{-4} psi (2 Pa) below ambient and near negligible in the fresh food compartment. There are a large number of paths for air flow and air leakage, including between the insulating foam and the outer and inner cabinet liners. Sealing a unit is very difficult. The unit does not hold pressure (and only small pressures of the order of the operating conditions) until essentially all the holes are sealed. Until that point the air simply finds another path to another leakage. Therefore, pressurization at relatively small pressure differences ~0.01 – 0.1 psi recommended as a means of finding the leakage points because soap water can be used and the leakages visualized via the formation of soap bubbles. A thermal imaging camera can also be used to help detect leakages but is not necessary. Air flows are predominantly cyclic with air mass inside of the cabinet increasing during compressor operation as the internal temperature decreases. This causes the air to become denser and therefore the cabinet gains air mass. After compressor operation the heavy air then "falls" back out of the cabinet. The cabinet is essentially "breathing;" "inhaling" air in during compressor operation, then "exhaling" air while the compressor is off.

If all leakages were completely sealed and the cycle thermostat set points remained the same the change in pressure between the cabinet and ambient would create forces of at least 300+ lbf on the fresh food door and at least 150 lbf on the freezer door from outside!

Therefore, while energy can be saved by better sealing the unit eventually pressure differences will become problematic as the leakages decrease.

4. CONCLUSION

In the presented study, the heat loss due to the gasket region and the air leakage attributed to a domestic refrigerator were experimentally investigated and evaluated.

The primary interest for the former study is measuring the heat leakage due to the defined gasket region in the unit of energy per unit time, per unit length along the gasket, per unit of temperature difference (w/m.K). To do so, a concept “Blue Box” was designed and built in order to isolate the heat transfer through the gasket region. Six heat flux sensor are installed along the outer surface of the exposed gasket region to measure the heat flux coming out of the box through this specific section. A number of thermocouples are responsible for getting temperature measurement over the experiments from box interior and ambient. There is a heater located inside the box which is used for adjusting the desired temperature difference across the gasket section. However, the heat flux sensors do not have enough resolution to resolve all surface heat flux distribution; therefore, 2D Computational Fluid Dynamics simulations are performed to provide the shape factors of the surface heat flux. The provided shape profile can be fit to the experimental data. Afterwards, the fitted shape profile can be integrated to provide us with the heat leakage in the unit of energy per unit time per unit length (w/m). Then, dividing this value by the temperature existing across the gasket region leads to the heat leakage in the interested unit (W/m.K). The heat leakage due to the gasket region in fresh-food compartment is estimated to be about 14% of the total thermal load. This value increased to 17% for the freezer compartment due to the higher temperature difference existing between the freezer interior and outside word.

Fresh food compartment	
Heat Leakage	0.20 (W/m.K)
Gasket Length	3.4 (m)
ΔT	20 (℃)
P_{loss}	13.6 (W)
$P_{Compressor}$	95 (W)
Gasket heat loss	14%

Table 4.1: Heat loss due to the gasket region in fresh food compartment of the sample refrigerator

Freezer compartment	
Heat Leakage	0.20 (W/m.K)
Gasket Length	2.4 (m)
ΔT	35 (℃)
P_{loss}	16.8 (W)
$P_{Compressor}$	95 (W)
Gasket heat loss	17%

Table 4.2: Heat loss due to the gasket region in freezer compartment of the sample refrigerator

The former research was defined on identifying the major air leakage paths and evaluating the air turn-over rate for freezer and fresh-food compartments with new gaskets installed. The pressure difference between each compartment and ambient was measured over the compressor operation and idle time on a sample refrigerator. Water drain tube and gasket are identified as primary paths for the air leakage. To measure the air turn over, the

unit should be completely sealed such that it can hold a pressure inside. However, it is a difficult procedure to seal all the air leakages. Actually, there are a large number of paths for the air to leak while the doors are closed. The unit does not hold any pressure until all the leakages are sealed. To detect the paths, it is recommended to pressurize the unit at a relatively small pressure difference, say 0.1 psi, so that it provides enough pressure at each air leakage path to let the bubbles appear when the soup water apply. Also, a thermal camera can be helpful to detect the air leakage paths, but is not necessary. Once the unit is sealed, a hole should be drilled through the wall of the fresh food compartment and the diameter has to be adjusted to match the originally measured pressure differences while the unit is operating. Note that the water drain tube is left open over the measurements. This creates a single-inlet, single outlet (SISO) system amenable to energy calculation. Next, flow rates and temperature are measured at the specified inlet and outlet. Having two temperatures and the mass flow rates at the inlet and outlet, the energy leakage due to the air infiltration can be calculated. The effective heat transfer rate due to air infiltration is calculated approximately 4.4 W which is about 4.6% of the total energy. Similarly, the actual air infiltration rates are ≈ 0.1 liters/min on a flow meter scaled from 0 – 15 liters / min.

Energy Loss due to Air Infiltration	
$\boldsymbol{P_{loss}}$	4.4 (W)
$\boldsymbol{P_{loss}}$	95 (W)
Air infiltration heat loss rate	4.6%

Table 4.3: Heat loss due to the air infiltration

APPENDICES

Appendix A

Quantitative Time Averaged Data

Table A.1: Measured heat flux running through the exposed gasket region for the expriment#1, Original gasket, $\Delta T = 20.2℃$, $\Delta T_{rms} = 0.148℃$

Experiment 1 **Gasket: Original** **Heat load : 9.20 W** $\Delta T = 20.2\ ℃$ ΔT_{rms}**= 0.148℃** **Heat leakage = 0.19 W/m.K**		
Sensor	**Mean Heat Flux (W/m^2)**	**RMS Heat Flux (W/m^2)**
HFS 1	**17.3**	**1.94**
HFS 2	**12.2**	**1.55**
HFS 3	**4.76**	**1.06**
HFS 4	**8.57**	**0.71**
HFS 5	**19.7**	**1.31**
HFS 6	**20.5**	**0.6**

Table A.2: Measured heat flux running through the exposed gasket region for the expriment#2, Original gasket, $\Delta T = 26.6℃$, $\Delta T_{rms} = 0.01℃$

Experiment 2 **Gasket:** **Heat load : 13.14 W** $\Delta T = 26.6℃$ ΔT_{rms}**= 0.01℃** **Heat leakage = 0.20 W/m.K**		
Sensor	**Mean Heat Flux (W/m^2)**	**RMS Heat Flux (W/m^2)**
HFS 1	**25.2**	**2.58**
HFS 2	**18.3**	**2.04**
HFS 3	**7.79**	**1.72**
HFS 4	**11.2**	**0.59**
HFS 5	**25.7**	**0.78**
HFS 6	**26.3**	**0.60**

Table A.3: Measured heat flux running through the exposed gasket region for the expriment#3, Original gasket, $\Delta T = 34.6℃$, $\Delta T_{rms} = 0.03℃$

Experiment 3 **Gasket:** **Heat load : 18.13 W** **$\Delta T = 34.6$ ℃** **$\Delta T_{rms} = 0.03$ ℃** **Heat leakage = 0.21 W/m.K**		
Sensor	**Mean Heat Flux (W/m^2)**	**RMS Heat Flux (W/m^2)**
HFS 1	**33.4**	**3.23**
HFS 2	**24.0**	**2.43**
HFS 3	**10.6**	**2.35**
HFS 4	**15.7**	**0.76**
HFS 5	**36.1**	**1.61**
HFS 6	**39.9**	**1.31**

Table A.4: Example measured heat flux running through the exposed gasket region for the expriment#1, Original gasket, $\Delta T = 25.2℃$

Experiment 4 **Gasket: Black –Side by Side** **Heat load : 13.14 W** **$\Delta T = 25.2$ ℃** **$\Delta T_{rms} =$** **Heat leakage = 0.23 W/m.K**		
Sensor	**Mean Heat Flux (W/m^2)**	**RMS Heat Flux (W/m^2)**
HFS 1	**24.86**	**3.20**
HFS 2	**18.06**	**2.15**
HFS 3	**7.13**	**1.24**
HFS 4	**10.65**	**0.93**
HFS 5	**27.02**	**2.39**
HFS 6	**30.46**	**1.51**

Table A.5: Example measured heat flux running through the exposed gasket region for the expriment#1, Original gasket, $\Delta T = 25.6℃$, $\Delta T_{rms} = 0.11℃$

Experiment 5 **Gasket: White** **Heat load : 13.14 W** $\Delta T = 25.6$ ℃ $\Delta T_{rms} = 0.11$℃ **Heat leakage = 0.22 W/m.K**		
Sensor	**Mean Heat Flux (W/m^2)**	**RMS Heat Flux (W/m^2)**
HFS 1	**24.9**	**2.88**
HFS 2	**17.6**	**2.28**
HFS 3	**7.46**	**1.45**
HFS 4	**10.5**	**1.52**
HFS 5	**24.8**	**1.69**
HFS 6	**27.3**	**1.43**

Appendix B

FORTRAN Code for Least Square Error Analysis

```
      PROGRAM FIT
      PARAMETER(N=6,M=100,NMAX=1000)
      real*8 X(N),Y(N),lms(NMAX)
      real*8 dlta,maxa,mina,error,minerror
      integer minnumber
      mina=0.2d+00
      maxa=2.d+00
      dlta=(maxa-mina)/dble(float(NMAX-1))
C Input the six experimental heat flux measurements
      X(1)=17.35
      X(2)=12.22
      X(3)=4.76
      X(4)=8.57
      X(5)=19.70
      X(6)=20.54
C Input the CFD curve values at the same locations
      Y(1)=19.66
      Y(2)=11.44
      Y(3)=8.15
      Y(4)=7.82
      Y(5)=19.93
      Y(6)=25.06
```

```
do j=1,NMAX
a=mina+dlta*dble(float(j-1))
lms(j)=0.d+00
error=0.d+00
do i=2,N
error=(X(i)-a*Y(i))*(X(i)-a*Y(i))
lms(j)=lms(j)+error
enddo
enddo
do j=2,N
lms(j)=lms(j)/float(N)
end do
minerror=999.d+00
do j=1,NMAX
if(minerror.gt.lms(j))then
minerror=lms(j)
minnumber=j
endif
enddo
print*,minerror,minnumber,mina+dlta*dble(float(minnumber-1))
pause
end
```

REFERENCES

1. Gupta, J.K., Ram Gopal M., and Chakraborty, S., Modeling of a domestic frost-free refrigerator. International Journal of Refrigeration, 30 (2007) 311-322.

2. Brent, T. Griffith, D.A., Turler D., Energy efficiency improvements for refrigerator/freezers using prototype doors containing gas-filled insulating systems. Proceedings of the 46 the International Appliance Technical Conference, USA, 15-17 May, 1995.

3. Xie, G., and Bansal, P.K., Analysis of defrosted water evaporation from three water trays in refrigerators. Applied Thermal Engineering, 20 (2000) 651-669.

4. Hasanuzzaman, M., and Saidur, R., and Masjuki, H.H., Effects of operating variables on heat transfer and energy consumption of a household refrigerator-freezer during closed door operation. Energy. 34 (2009) 196-198.

5. Boughton, B.E., and Clausing, A.M., and Newell T.A., Investigation of household refrigerator cabinet thermal loads. HVAC and R Research, (1996) 135-148.

6. Shapiro, N. and Ghasemmi, M, Review of energy efficiency of refrigerator/freezer gaskets. Environmental Protection Agency, EPA/600/S2-91/060, 1991.

7. Hessami, M.A., and Hilligweg, A., Energy Efficient Refrigerators: The effect of door gasket and wall insulation on heat transfer. 2003. ASME.

8. Tao, W.H. and Sun, J. Y., Simulation and experimental study on the air flow and heat loads of different refrigerator cabinet designs. Chemical Engineering Communications. 186(20011): p. 171-182.

9. Bansal, P., Vineyard, E., Abdelaziz, O., Advances in household appliances -a review. Applied Thermal Engineering. 31(2011) 3748-60

10. Sim, J.S. and Ha, J.S., A study on the heat transfer characteristics for the refrigerator by using reverse heat load method. International Communications in Heat and Mass Transfer. 38 (2011) 572-576

11. Kim, H.S., and Sim, J.S., and Ha, J.S. A study on the heat transfer characteristics near the magnetic door gasket of a refrigerator. International Communications in Heat and Mass Transfer, 38 (2011) 1226-1231

12. Labat, M., and Woloszyn, M., Assessment of the air change rate of airtight buildings under natural conditions sing the tracer gas technique. Comparison with numerical modelling. Building and Environment 60 (2013) 37-44

13. Amin, M. and Navaz, K., Tracer gas technique: A new approach for steady state infiltration rate measurement of open refrigerated display cases. Journal of Food Engineering 92 (2009) 172–181

14. Foster, A., Barrett, R., James, S.J. and Swain, M.J., Measurement and prediction of air movement through doorways in refrigerated rooms. International journal of refrigeration, 25(8): p. 11(2002)-1109.

15. Buggenhouta, S. and Van Brecht, A., Influence of sampling positions on accuracy of tracer gas measurements in ventilated spaces. Bio System Engineering 104(2009) 216–223

16. Huelsz, G. and Gómez, F., Pineirua, M., Rojas, J., Alba, M., Guerra, V., , Evaluation of refrigerator/freezer gaskets thermal loads, HVAC&R Research, 17(2011):2, 133-143

17. Afonso C. and Castro M., Air infiltration in domestic refrigerators: The influence of the magnetic seals conservation. International Journal of Refrigeration. 33(2010)856-567

18. Melo, C. and Silva, L. W. da; and Pereira, R. H., Experimental evaluation of the heat transfer through the walls of household refrigerators (2000). International Refrigeration and Air Conditioning Conference. Paper 502.

19. Stein, M.A., Inan, C., Bulllard, C., Newell, T., Closed door moisture transport in refrigerator/freezer, International Journal of Energy Research; 26 (2002) 793–805

20. Diller, T.E. et al., Experimental performance of a heat flux micro-sensor, ASME, 113 (2002), 246-250

21. Haitao, L. and Dan, S., Theory analysis of thermocouple temperature measurements, Applied Mechanics and Materials (2013) pp 749-753

22. Gao, F. master's thesis Numerical simulation of the heat leakage at the gasket region of domestic refrigerator, December 2014.